Tropical cyclone integrated kinetic energy in an ensemble of HighResMIP simulations

Article

Accepted Version

Kreussler, P. ORCID: https://orcid.org/0000-0003-4328-4712, Caron, L.-P. ORCID: https://orcid.org/0000-0001-5221-0147, Wild, S. ORCID: https://orcid.org/0000-0002-1089-5579, Tomas, S. L., Chauvin, F. ORCID: https://orcid.org/0000-0001-6071-7212, Moine, M.-P., Roberts, M. J., Ruprich-Robert, Y., Seddon, J. ORCID: https://orcid.org/0000-0003-1302-1049, Valcke, S. ORCID: https://orcid.org/0000-0002-0438-5978, Vannière, B. and Vidale, P. L. ORCID: https://orcid.org/0000-0002-1800-8460 (2021) Tropical cyclone integrated kinetic energy in an ensemble of HighResMIP simulations. Geophysical Research Letters, 48 (5). e2020GL090963. ISSN 1944-8007 doi: 10.1029/2020gl090963 Available at https://centaur.reading.ac.uk/96719/

To link to this article DOI: http://dx.doi.org/10.1029/2020gl090963

Publisher: American Geophysical Union (AGU)

Tropical Cyclone Precipitation in the HighResMIP Atmosphere-only Experiments of the PRIMAVERA Project

Wei Zhang[1,2*], Gabriele Villarini[1], Enrico Scoccimarro[3], Malcolm Roberts[4], Pier Luigi Vidale[5], Benoıt Vanniere[5], Louis-Philippe Caron[6], Dian Putrasahan[7], Christopher Roberts[8], Retish Senan[8], and Marie-Pierre Moine[9]

[1] IIHR-Hydroscience & Engineering, The University of Iowa, Iowa City, Iowa, USA

[2]Department of Plants, Soils and Climate, Utah State University, Utah, USA

[3] Fondazione Centro Euro-Mediterraneo sui Cambiamenti Climatici, Bologna, Italy

[4] UK Meteorological Office, Exeter, UK

[5]National Centre for Atmospheric Science (NCAS), Department of Meteorology, University of Reading, Reading, UK

[6]Barcelona Supercomputing Center (BSC), Barcelona, Spain

[7]Max Planck Gesellschaft zur Foerderung der Wissenschaften E.V. (MPI-M), Hamburg, Germany

[8]European Centre for Medium-Range Weather Forecasts (ECMWF), Reading, UK

[9]Climat, Environnement, Couplages, Incertitudes (CECI), Universit´e de Toulouse, CNRS, Cerfacs, Toulouse, France

Revision submitted to

Climate Dynamics

*Corresponding author:

Wei Zhang, Ph.D.
Department of Plants, Soils and Climate, Utah State University, Utah, USA.
Email: w.zhang@usu.edu
Phone: (435) 791-1101

Abstract

This study examines the climatology and structure of rainfall associated with tropical cyclones (TCs) based on the atmosphere-only Coupled Model Intercomparison Project Phase 6 (CMIP6) HighResMIP runs of the PRocess-based climate sIMulation: AdVances in high resolution modelling and European climate Risk Assessment (PRIMAVERA) Project during 1979-2014. We evaluate how the spatial resolution of climate models with a variety of dynamic cores and parameterization schemes affects the representation of TC rainfall. These HighResMIP atmosphere-only runs that prescribe historical sea surface temperatures and radiative forcings can well reproduce the observed spatial pattern of TC rainfall climatology, with high-resolution models generally performing better than the low-resolution ones. Overall, the HighResMIP atmosphere-only runs can also reproduce the observed percentage contribution of TC rainfall to total amounts, with an overall better performance by the high-resolution models. The models perform better over ocean than over land in simulating climatological total TC rainfall, TC rainfall proportion and TC rainfall per TC in terms of spatial correlation. All the models in the HighResMIP atmosphere-only runs underestimate the observed composite TC rainfall structure over both land and ocean, especially in their lower resolutions. The underestimation of rainfall composites by the HighResMIP atmosphere-only runs is also supported by the radial profile of TC rainfall. Overall, the increased spatial resolution generally leads to an improved model performance in reproducing the observed TC rainfall properties.

1. Introduction

Tropical cyclones (TCs) are associated with extreme rainfall and are responsible for extensive damages and numerous fatalities (e.g., Peduzzi et al. 2012; Rappaport 2014; Czajkowski et al. 2017; Klotzbach et al. 2018; Bosma et al. 2020). For example, Hurricanes Harvey and Florence serve to highlight the catastrophes that could be caused by extreme TC rainfall (e.g., Emanuel 2017; Reed et al. 2018; Risser and Wehner 2017; Van Oldenborgh et al. 2017; Wang et al. 2018; Zhang et al. 2018) and are just two recent examples of a long list of catastrophic events. According to the National Oceanic and Atmospheric Administration (NOAA) National Center for Environmental Information (NCEI) (2020), there have been 44 TCs affecting the United States causing damage in excess of one billion dollars between 1980 and 2019; in total, these events caused $945.9B (Consumer Price Index-Adjusted) and 6,502 fatalities.

Rainfall associated with TCs tends to be larger than for non-TC events. For instance, within the novel statistical framework of the Metastatistical Extreme Value Distribution, Miniussi et al. (2020) showed that the distribution of TC rainfall is different from the non-TC rainfall in the Eastern United States, especially for multi-day events, and that these storms tend to result in larger rainfall values. The impact of the TC rainfall is remarkable not only along the coastline, but also hundreds of miles inland in terms of flooding (e.g., Villarini et al. 2014a; Khouakhi et al. 2017; Aryal et al. 2018) and landslides (e.g., Bucknam et al. 2001). Despite these negative effects, they can also bring water critical for groundwater recharge, water supply and drought mitigation (e.g., Abdalla and Al-Abri 2011; Kam et al. 2013; Zhang et al. 2017). It is therefore crucial that we improve our understanding of the processes and characteristics of TC rainfall, which could in turn lead to an improvement in its simulation and seasonal forecasting (e.g., Barlow 2011; Luitel et al.

2018; Liu et al. 2019; Prat and Nelson, 2016; Touma et al. 2019; Vecchi et al. 2019; Zhang et al. 2019).

There are several drivers controlling TC rainfall, including low-level vertical wind shear (Corbosiero and Molinari 2003; Tang et al. 2014), terrain effects (DeHart and Houze Jr 2017; Nguyen et al. 2017), TC structure (Chen et al. 2006; Hence and Houze Jr 2012; Yu et al. 2017), sea surface temperature (Langousis and Veneziano 2009; Lin et al. 2015), and atmospheric aerosols (Wang et al. 2014; Zhao et al. 2018). Over the years and thanks to advances in observing capabilities, major progress has been made in understanding the temporal and spatial components of TC rainfall through satellite monitoring (e.g., Rios Gaona et al. 2018; Jiang and Zipser 2010; Jiang et al. 2011; Prat and Nelson 2013b), radar data (e.g., Villarini et al. 2011; Bao et al. 2017; Janapati et al. 2020) and rain gauges (e.g., Khouakhi et al. 2017; Villarini and Denniston 2016). Overall, these studies indicate that TC rainfall substantially contributes to the mean and extreme precipitation events, particularly along coastal regions (Khouakhi et al. 2017; Shepherd et al. 2007; Knight et al. 2009; Prat et al. 2013; Villarini et al. 2011; 2014b). In addition to observations, numerical models with the capability of resolving TCs have been used to examine TC rainfall (e.g., Daloz et al. 2010; Kim et al. 2018; Liu et al. 2018; 2019; Moon et al. 2020; Scoccimarro et al. 2014; 2017a; Villarini et al. 2014; Zhang et al. 2019). While climate models can well simulate the overall climatology of TC rainfall (e.g., Zhang et al. 2019), these models have limitations in simulating individual events and exhibit strong discrepancies in the simulated pattern and magnitude of TC rainfall (Scoccimarro et al. 2017c; Wright et al. 2015; Zhang et al. 2019).

In the climate modeling community, special attention has been paid to the examination of the impacts of horizontal resolution on TC simulations (e.g., Zhao et al. 2009; Caron et al. 2011; Manganello et al. 2012; Wehner et al. 2014; Roberts et al. 2015; 2020; Murakami et al. 2015;

Zhang et al. 2015; Vecchi et al. 2019). Despite these efforts, it is difficult to generalize the conclusions of these studies because of the differences in experimental design, tracking algorithm, and model parameters. While much of the focus has been on the role of resolution in terms of TC characteristics, recently Zhang et al. (2019) assessed the role of horizontal resolution of two climate models (i.e., the Geophysical Fluid Dynamics Laboratory (GFDL) Forecast-Oriented Low Ocean Resolution version of CM2.5 (FLOR, ~50km) and the High-Resolution FLOR (HiFLOR, ~25km)) in simulating TC rainfall and found that the high-resolution model (~25km) outperforms the low-resolution model (~50km) in reproducing and forecasting TC rainfall.

Based on this overview, numerical models have advanced our understanding of TC rainfall and provided insights into future projection of TC rainfall; however, there is a very limited number of climate models that can properly resolve TCs. Although there are individual studies that have focused on the impacts of horizontal resolution on TCs, there are many differences in the models' setups and simulations that would lead to the different behaviors in simulating TC rainfall, representing a critical obstacle in terms of the generalization of the results from different studies. Most conclusions drawn on the projection of TC rainfall are based on the fifth phase of the Coupled Model Intercomparison Project (CMIP5)'s climate models with spatial resolution of ~1-3 degrees, which are too coarse to properly resolve TCs. To overcome this limitation, the sixth phase of the Coupled Model Intercomparison Project (CMIP6) High Resolution Model Intercomparison Project (HighResMIP) provides multi-model and multi-resolution simulations to the scientific community (Haarsma et al. 2016). Using the CMIP6 HighResMIP protocol, the European Union Horizon 2020's PRocess-based climate sIMulation: AdVances in high resolution modelling and European climate Risk Assessment (PRIMAVERA) project has contributed global atmospheric general circulation models (AGCM) simulations at a CMIP6-type resolution (i.e., ~100 km) and higher (e.g., ~25 km), which allow us to examine TCs and understand the robustness of changes in TC rainfall across a wide range of numerical models and spatial resolutions (Roberts et al. 2020). Roberts et al. (2020) examined the roles of horizonal resolution in simulating TCs in terms of frequency, intensity, structure and accumulated cyclone energy across these models. In addition, Vanniere et al. (2020) focused on the sensitivity of moisture budget associated with TC rainfall to different spatial resolution of the climate models in this project. This study will take advantage of the simulations archived in the PRIMAVERA project to evaluate the fidelity of these climate models in representing TC rainfall and the dependence of skill on resolution.

The remainder of the manuscript is organized as follows. Section 2 describes data and methods, followed by Section 3 that presents results based on observations and models. Finally, Section 4 summarizes the main points and concludes the study.

2. Data and Methods

TC observations are obtained from the International Best Track Archive for Climate Stewardship (IBTrACS) version 4 with longitude, latitude, time, intensity (i.e., maximum sustained wind) and central pressure at the six-hour time scale (Knapp et al. 2010). Rainfall is obtained from the Multi-Source Weighted-Ensemble Precipitation, version 2 (MSWEP V2) which is a gridded precipitation dataset available during 1979–2017 with high spatial (0.1°) and temporal (three-hour) resolution (Beck et al. 2017a,b). TC rainfall is defined as the rainfall at 6-hour intervals within a 500-km radius of a TC center by accounting for the rainfall covering the inner core of the TC and the adjacent rainbands (e.g., Dare et al. 2012; Villarini et al. 2014b; Zhang et al. 2019). Although there might be some uncertainties in extracting TC rainfall using this radius at each 6-hour time step, the selection of this radius is also supported by the fact that most precipitation associated with TCs occurs within 5° (~500km) from the center of the storm for climate models (Trenberth et al. 2007; Vanniere et al. 2020). The TC-rainfall composites are the composites of the extracted TC rainfall using the 500-km radius and we process the TC rainfall for three scenarios: land and ocean, only land and only ocean.

We use the HighResMIP atmosphere-only simulations performed by the Met Office Hadley Centre's HadGEM3-GC313-GC31 (Roberts et al. 2019a), the European Centre for Medium-Range Weather Forecasts Integrated Forecasting System (ECMWF IFS) (Roberts et al. 2018), CNRM-CM6-1 developed by Centre National de Recherches Météorologiques—Groupe d'études de l'Atmosphère Météorologique/Centre Européen de Recherche et de Formation Avancée (Voldoire et al. 2019), the Fondazione Centro Euro-Mediterraneo sui Cambiamenti Climatici Climate Model Version 2 (CMCC-CM2-(V)HR4; Cherchi et al. 2019, Scoccimarro et al. 2020), the EC-EARTH3 Consortium's EC-Earth3P (Haarsma et al. 2019), and Max Planck Institute Earth System Model version 1.2 (MPI-ESM1-2; Gutjahr et al. 2019) (see Table 1 for details). The atmosphere-only HighResMIP experiments are forced by the historical estimates of sea surface temperature, sea ice, and radiative forcings (as described in Haarsma et al. 2016). It should be noted that the atmosphere-only HighResMIP simulations are slightly different from the CMIP6 (Eyring et al. 2016) AMIP experiments (Gates et al. 1999) in terms of forcing of aerosol, sea surface temperature and sea ice (Roberts et al. 2020). We obtain the model simulations archived in the Earth System Grid Federation (ESGF) nodes, including Roberts (HadGEM3-GC31; 2017a, 2017b, 2017c), Roberts et al. (ECMWF-IFS; 2017a, 2017b), Voldoire (CNRM-CM6-1; 2017, 2018), Scoccimarro et al. (CMCC-CM2-(V)HR4; 2017b, 2017c), EC-Earth Consortium (EC-Earth3P; 2018a, 2018b), and von Storch et al. (MPI-ESM1-2; 2017, 2019). In addition, the TC tracks obtained from these datasets are available from Roberts (2019b).

To facilitate the comparison of the simulation of TC rainfall, the climate model outputs are grouped into high-, medium- and low- spatial-resolution models (Table 1). While ECMWF IFS data provided to the HighResMIP simulations are based on a reduced-resolution regular grid, the original ECMWF-IFS output uses the cubic octahedral reduced Gaussian grid, with resolutions of Tco399 (~25 km) and Tco199 (~50 km) for the HR and LR configurations, respectively. Therefore, we include ECMWF-IFS-HR/ECMWF-IFS-LR in the high-resolution/middle-resolution group, respectively (Table 1). TC tracks with latitude, longitude, time and intensity are derived by applying a tracker called "TRACK" to the simulations performed by these models (Hodges et al. 2017). This tracker uses the 6-hourly relative vorticity at the 850-, 700-, and 600-hPa levels for tracking TCs and has been widely used in TC studies (Hodges et al. 2017).

We evaluate the performance of these models in simulating TC rainfall across the globe, and for the basins (Table 2): western North Pacific, eastern North Pacific, North Atlantic, South Atlantic, North Indian Ocean, South-West Indian Ocean and South Pacific & Australia. We use spatial correlation and root mean square error (RMSE) as quantitative metrics for the evaluation. Because there is no named storm in South Atlantic in observations during the study period (Table S1), we do not include the analysis of spatial correlation and RMSE between observations and models for this basin.

Beyond the high resolution of these models, a major advantage of the PRIMAVERA Project is the consistency of the simulations and outputs: all the models were run using the same forcings, and the tracking of the storms is the same across models, allowing for a direct comparison in terms of model performance and on the role of resolution.

3. Results

3.1 Total TC rainfall

The annual total TC rainfall averaged over 1979-2014 in the observations exhibits regional differences across ocean basins (Figure 1). For example, the annual TC rainfall is the highest in the western North Pacific, followed by the eastern North Pacific. The annual TC rainfall in the North Atlantic is lower than in the eastern North Pacific and little TC rainfall is observed in the South Atlantic (Figure 1). Qualitatively, the climate models tend to capture the overall spatial climatological pattern of TC rainfall in the observations; this is particularly true in relation to the areas in the North Pacific characterized by larger TC rainfall values compared to the rest of the basins (Figure 2). The GCMs generally produce spurious TC rainfall in the South Atlantic (Figure 2). Specifically, CMCC-CM2-VHR4, EC-Earth3P-HR, ECMWF-IFS-HR, and ECMWF-IFS-LR reproduce well the total TC rainfall amount across different basins (Figure 2), consistent with spatial correlation and RMSE between observed and simulated total TC rainfall (Tables 3-4). In addition, CNRM-CM6-1-HR, CNRM-CM6-1, HadGEM3-GC31-HM, HadGEM3-GC31-MM, HadGEM3-GC31-LM point to an overestimation of the total TC rainfall, while EC-Earth3P, MPIESM1-2-XR and MPIESM1-2-HR to an underestimation of the total TC rainfall across all basins (Figure 2). This is consistent with the results of TC track density (Figure 3), which is also documented in Roberts et al. (2020) which reported that EC-Earth3P and MPIESM1-2-XR underestimate TC track density. Vanniere et al. (2020) also found that TC activity/frequency plays an important role in explaining the differences in total TC rainfall between high-resolution and low-resolution models. Based on the above results, high-resolution models tend to perform better in reproducing the observed climatology of TC rainfall. Overall, increase in model resolution tends to produce a higher amount of total TC rainfall for the CMCC models, EC-Earth3P models, HadGEM3-GC31 (i.e., HadEM3-GC31-HM and HadGEM3-GC31-LM) and ECMWF-IFS models, while TC rainfall shows little to no sensitivity to spatial resolution in CNRM-CM6-1 and MPIESM1-2 models (Figure 2). Four of the six models exhibit remarkable differences in TC rainfall between high-resolution and low-resolution models while the other two show similar results (Figure 2). The low sensitivity to spatial resolution in CNRM-CM6-1 and MPIESM1-2 models may be due to low absolute resolution in the models, the high-resolution version of which is around ~50km (Table 1).

3.2 Contribution of TC rainfall to Total Rainfall

In addition to total TC rainfall, we also examine the percentage contribution of TC rainfall to total rainfall. In the observations, the percentage contribution presents remarkable regional differences with the highest values in the western and eastern North Pacific (Figure 4), consistent with total TC rainfall (Figure 1). Climate models exhibit strong discrepancies in the capability of reproducing the observed percentage contribution (Figure 4). Globally, EC-Earth3P-HR, ECMWF-IFS-HR, ECMWF-IFS-LR, HadGEM3-GC31-HM, HadGEM3-GC31-MM, and HadGEM3-GC31-LM reproduce well the observed contribution of TC rainfall in terms of RMSE. CMCC-CM2-VHR4, EC-Earth3P-HR, EC-Earth3P, ECMWF-IFS-HR, ECMWF-IFS-LR, and HadGEM3-GC31 models produce spatial correlations greater than 0.8, suggesting a good performance (Table 5). The models exhibit marked regional differences. For example, CNRM-CM6-1-HR and CNRM-CM6-1 reproduce well the observed contribution of TC rainfall in the western North Pacific, and the performance of these models is not very promising in the North Indian Ocean (Figure 4 and Tables 5-6). High-resolution models generate a higher contribution, more similar to the observations except for MPIESM1-2-XR/MPIESM1-2-HR and CNRM-CM6-1-HR/CNRM-CM6-1, which produce similar percentage contributions between high-resolution and low-resolution models (Figure 4). Therefore, most of the high-resolution models perform better than their low-resolution counterparts in reproducing the global fractional contribution (Figure 4 and Table 5). To further understand the proportion of TC rainfall, we also examine the bias in the models (Figure 5). Overall, the bias in TCR proportion (Figure 5) is mainly due to the bias in TC rainfall (Figure 2), rather than total precipitation (Figure 6).

3.3 TC rainfall per track density

All the models in the PRIMAVERA Project underestimate the amount of TC rainfall per track density (i.e., total TC rainfall divided by track density) in the observations (Figure 7). Therefore, given that the TC rainfall amounts identified in the models were similar to the observations, it means that there are generally more storms in the models than in the observational records. As we compare the results between the different resolutions of the models, some models (i.e., CMCC-CM2, CNRM and HadGEM3-GC31) have a tendency for lower-resolution versions to have larger per-TC rainfall amounts. This counter-intuitive results may be due to the fact that lower TC density is produced by low-resolution simulations than in the high-resolution ones (Figure 3), consistent with Vanniere et al. (2020) showing that rainfall per TC is biased high in low-resolution models. The spatial correlation between observed and simulated amount of TC rainfall per track density (Table S2) is lower than for total TC rainfall or fractional contribution, with most of the correlation coefficients that are not statistically significant. Among the models used in this study, the CNRM models perform the best in simulating the rainfall per track density (Figure 7 and Tables S2-3) and this is consistent with the fact that CNRM performs well in simulating the strongest TCs (Roberts et al. 2020).

3.4 TC rainfall over Ocean and Land

We also evaluate the performance of the models in simulating climatological TC rainfall over ocean and land. Overall, the models perform better in simulating total TC rainfall, TC rainfall proportion and TC rainfall per TC over ocean than over land in terms of spatial correlation (Tables S4-6). However, the models generate a larger RMSE for the three metrics over ocean than over land (Tables S4-6), and this may be due to a large climatology of TC rainfall over ocean (Figure 1).

3.5 Composites and Profile of TC rainfall

We process the composite TC rainfall (within the 500-km radius of TC center) at 6-hour time step for all the storms, those in the northern hemisphere and those in the southern hemisphere in observations and climate models (Figure 8). The composite TC rainfall (within the 500-km radius) at 6-hourly intervals in the observations is higher than model simulations over ocean and land (Figure 8). CMCC-CM2-VHR4 performs the best in reproducing the composite TC rainfall over ocean and land, with larger precipitation values closer to the center of circulation of the storms, even though the size of the TCs tends to be smaller than in the observations and in other models (e.g., CNRM). There is also a tendency for the storms in the northern hemisphere to exhibit larger rainfall values compared to those in the southern hemisphere, consistent with the observations. The high-resolution models produce larger composite TC rainfall rate than low-resolution models, which tend to spread rainfall over larger distances from the center of circulation of the TCs (Figure 8). In addition, we compare the composite rainfall in the 200 strongest storms in observations and the low- and high-resolution models. Overall, the composite rainfall rate in the high-resolution models is larger than in the low-resolution ones except for the MPI-ESM 1-2 models that simulate similar composite TC rainfall (Figure 9). The differences in composite TC rainfall of the 200 strongest TCs between low-resolution and high-resolution models (Figure 9) are more remarkable than the results for all TCs (Figure 8), and this may be due to a large portion of intense TCs in the high-resolution models than low-resolution ones (Roberts et al. 2020). To assess whether the models' skill is different in simulating TC rainfall over ocean or land mass, we examine the composite TC rainfall over ocean and land, separately. The composite TC rainfall over the ocean exhibits similar characteristics as those over land & ocean, with a well-defined center of circulation, albeit presenting a slightly higher magnitude (Figure 10). While almost all the models underestimate the composite TC rainfall over land compared with observations (Figure 11), CMCC-CM2-VHR4 slightly overestimates the center of composite TC rainfall over land and HadGEM3-GC31-HM produces a similar magnitude of composite TC rainfall over land (Figure 11). Given the fact that TCs in models have a shorter path on land than the observations (due to the tracker) and TC rainfall rate over ocean is larger than over land, this suggests that the underestimation of composite TC rainfall in models might be even more pronounced than the results here. Based on these results, there are no large differences in the performance of the models in reproducing composite TC rainfall over ocean or land. Note that the composite rainfall patterns are consistent with the results in Kim et al. (2018) which examined the composite TC rainfall across a family of Geophysical Fluid Dynamics Laboratory (GFDL) models.

In addition to the examination of the composite TC rainfall, we compute the radial profile of TC rainfall across different models grouped by spatial resolution (Table 1) and land/ocean masks (Figure 12). Consistent with the results in Figures 8-11, the observed rainfall tends to be higher than what is generated by these models, especially closer to their center of circulation; this statement is valid regardless of resolution, and whether over land or ocean. The observed TC rainfall over the oceans tends to peak within 100 km from the center of the storm, and then to rapidly decrease as we move further away. This feature is generally well captured by the models, with the CMCC-CM2-VHR4 tending to perform the best among high-resolution groups. Among the mid-resolution group, HadGEM3-GC31-MM exhibits the highest skill in simulating the radial profile of TC rainfall, while CNRM-CM6-1 tends to perform the best among the low-resolution group (Figure 12). The model performance in terms of TC rainfall when the storms are over land is similar to that mentioned for the storms over the ocean, even though the rainfall amounts tend to be smaller and to decrease more slowly as they progress inland. The radial profile of TC rainfall is consistent with Kim et al. (2018) and Moon et al. (2020) in terms of pattern and magnitude of TC rainfall across different climate models.

4. Conclusion

TC rainfall has been a challenge for climate modeling community because this metric is associated with TC genesis, track, and intensity. By taking advantage of the European Union Horizon 2020's PRIMAVERA Project, we have examined the skill of state-of-the-art global climate models in reproducing several aspects of the rainfall associated with these storms in HighResMIP atmosphere-only experiments and assessed the dependence of the skill on model resolution.

In general, high-resolution models perform better than their lower resolution counterparts in reproducing several characteristics of the TC distribution. They tend to provide a more realistic representation of the observations both in terms of patterns and amounts, except for average TC rainfall per track density for which low-resolution models seem better for some models. The simulation of TC rainfall by these models exhibits remarkable regional differences and discrepancies. For example, the CMCC-CM2 and ECMWF-IFS models reproduce the total TC rainfall found in observations, while they slightly underestimate their percentage contribution and overall amount per track density. By contrast, CNRM-CM6-1 and HadGEM3-GC31 models overestimate total TC rainfall, but they reproduce the fractional contribution of TC rainfall to total rainfall. MPIESM1-2 and EC-Earth3P models underestimate most of the metrics associated with TC rainfall. Overall, the models perform better in simulating climatological total TC rainfall, TC rainfall proportion and TC rainfall per TC over ocean than over land in terms of spatial correlation. However, the models generate larger RMSE for the three metrics over ocean than over land, probably due to a larger climatology of TC rainfall over ocean.

When we stratified the results of composite TC rainfall across land and ocean, we did not find any large changes in performance of these models, as they were able to reproduce the overall patterns albeit with lower rainfall magnitudes. Overall, CMCC-CM2-VHR4 performs the best in simulating the radial profile of TC rainfall among the high-resolution model group, while HadGEM3-GC31-MM (CNRM-CM6-1) exhibits the highest skill in simulating the radial profile of TC rainfall in the mid-resolution (low-resolution) group.

While most models tend to improve their performance as we increase their horizontal resolution, the CNRM-CM6-1 and MPIESM1-2 models are two exceptions, producing similar results in their low- and high- resolution versions. Such similar performances between high-resolution and low-resolution climate models need to be further investigated from the perspective of convection, circulation and TC dynamics. For example, Vanniere et al (2020) investigated possible mechanisms by examining moisture budget, and found that the distribution of precipitation per TC averaged in a 5-degree radial cap does not change significantly, which can be explained by the large-scale balance that shapes the moisture budget of TCs.

In summary, our findings indicate that the investment in performing the high-resolution simulations with these models has been paid off in terms of the gained realism in reproducing TC rainfall. As we increase the horizontal resolution and we improve the description of the processes at play, we expect to further improve the simulation of these storms, providing basic information towards our preparation, mitigation and response efforts.

Acknowledgetments:

We thank the two anomynous reviewers for insightful comments. Wei Zhang and Gabriele Villarini acknowledge support by the National Science Foundation under Grant EAR-1840742. MR, LPC, CDR, RS, PLV, ES, BV, DP, and MPM acknowledge funding from the PRIMAVERA project, funded by the European Union's Horizon 2020 programme under Grant Agreement no. 641727.

Reference:

Abdalla, O., and R. bin Y. Al-Abri, (2011). Groundwater recharge in arid areas induced by tropical cyclones: lessons learned from Gonu 2007 in Sultanate of Oman. Environ Earth Sci, 63, 229–239. https://doi.org/10.1007/s12665-010-0688-y

Aryal, Y.N., G. Villarini, W. Zhang, and G.A. Vecchi, Long term changes in flooding and heavy rainfall associated with North Atlantic tropical cyclones: Roles of the North Atlantic Oscillation and El Niño-Southern Oscillation, Journal of Hydrology, 559, 698-710, 2018.

Bao, X., D. Wu, X. Lei, L. Ma, D. Wang, K. Zhao, and B. J.-D. Jou, 2017: Improving the extreme rainfall forecast of Typhoon Morakot (2009) by assimilating radar data from Taiwan Island and mainland China. *Journal of Meteorological Research*, **31,** 747-766.

Barlow, M., 2011: Influence of hurricane-related activity on North American extreme precipitation. Geophysical Research Letters, 38 , L04705.

Beck, H. E., A. I. Van Dijk, V. Levizzani, J. Schellekens, D. Gonzalez Miralles, B. Martens, and A. De Roo, 2017a: MSWEP: 3-hourly 0.25 global gridded precipitation (1979-2015) by merging gauge, satellite, and reanalysis data. *Hydrology and Earth System Sciences*, **21,** 589-615.

Bosma, C. D., D. B. Wright, P. Nguyen, J. P. Kossin, D. C. Herndon, and J. M. Shepherd, 2020: An intuitive metric to quantify and communicate tropical cyclone rainfall hazard. Bulletin of the American Meteorological Society, 101, E206-E220.

Beck, H. E., and Coauthors, 2017b: Global-scale evaluation of 22 precipitation datasets using gauge observations and hydrological modeling. *Hydrology and Earth System Sciences*, **21,** 6201.

Bucknam, R. C., J.A. Coe, M.M. Chavarria, J.W. Godt, A.C. Tarr, … , and M.L. Johnson (2001). Landslides triggered by Hurricane Mitch in Guatemala - Inventory and discussion. USGS Report Number 2001-443.

Caron, L-P, CG Jones and K Winger (2011) Impact of resolution and downscaling technique in simulating recent Atlantic tropical cyclone activity. Climate Dynamics, 5, 869-892. doi: 10.1007/s00382-010-0846-7.

Chavas, D. R., N. Lin, W. Dong, and Y. Lin (2016), Observed Tropical Cyclone Size Revisited, *Journal of Climate*, *29*(8), 2923-2939, doi:10.1175/jcli-d-15-0731.1.

Chen, S. S., J. A. Knaff, and F. D. Marks Jr, 2006: Effects of vertical wind shear and storm motion on tropical cyclone rainfall asymmetries deduced from TRMM. *Monthly Weather Review*, **134,** 3190-3208.

Cherchi, A., and Coauthors, 2019: Global Mean Climate and Main Patterns of Variability in the CMCC-CM2 Coupled Model. *Journal of Advances in Modeling Earth Systems*, **11,** 185-209.

Corbosiero, K. L., and J. Molinari, 2003: The relationship between storm motion, vertical wind shear, and convective asymmetries in tropical cyclones. *Journal of the Atmospheric Sciences*, **60,** 366-376.

Czajkowski, J., G. Villarini, M. Montgomery, E. Michel-Kerjan, and R. Goska, Assessing current and future freshwater flood risk from North Atlantic tropical cyclones via insurance claims, Scientific Reports, 7, 1-10, 2017.

Daloz, A. S., F. Chauvin, and F. Roux, 2010: Tropical cyclone rainfall in the observations, reanalysis and ARPEGE simulations in the North Atlantic Basin. Hurricanes and climate change, Springer, 57-79.

Dare, R. A., N. E. Davidson, and J. L. McBride, 2012: Tropical cyclone contribution to rainfall over Australia. *Monthly Weather Review*, **140,** 3606-3619.

DeHart, J. C., and R. A. Houze Jr, 2017: Orographic modification of precipitation processes in Hurricane Karl (2010). *Monthly Weather Review*, **145,** 4171-4186.

EC-Earth Consortium (EC-Earth), 2018a: EC-Earth-858 Consortium EC-Earth3P model output prepared for CMIP6 HighResMIP. Earth System Grid Federation. http://cera860 www.dkrz.de/WDCC/meta/CMIP6/CMIP6.HighResMIP.EC-Earth-Consortium.EC861Earth3P

EC-Earth Consortium (EC-Earth), 2018b: EC-Earth-Consortium EC-Earth3P-HR model output prepared for CMIP6 HighResMIP. Earth System Grid Federation. http://cera-www.dkrz.de/WDCC/meta/CMIP6/CMIP6.HighResMIP.EC-Earth-Consortium.EC-Earth3P-HR

Emanuel, K., 2017: Assessing the present and future probability of Hurricane Harvey's rainfall. *Proceedings of the National Academy of Sciences*, **114,** 12681-12684.

Gates, W. L., and Coauthors, 1999: An overview of the results of the Atmospheric Model Intercomparison Project (AMIP I). *Bulletin of the American Meteorological Society*, **80,** 29-56.

Gutjahr, O., and Coauthors, 2019: Max Planck Institute Earth System Model (MPI-ESM1.2) for the High-Resolution Model Intercomparison Project (HighResMIP). *Geosci. Model Dev.*, **12,** 3241-3281.

Haarsma, R. J., and Coauthors, 2016: High Resolution Model Intercomparison Project (HighResMIP v1.0) for CMIP6. *Geosci. Model Dev.*, **9,** 4185-4208.

Hence, D. A., and R. A. Houze Jr, 2012: Vertical structure of tropical cyclone rainbands as seen by the TRMM Precipitation Radar. *Journal of the atmospheric sciences*, **69,** 2644-2661.

Hodges, K., A. Cobb, and P. L. Vidale, 2017: How well are tropical cyclones represented in reanalysis datasets? *Journal of Climate*, **30,** 5243-5264.

Janapati, J., and Coauthors, 2020: Raindrop Size Distribution Characteristics of Indian and Pacific Ocean Tropical Cyclones Observed at India and Taiwan Sites. *Journal of the Meteorological Society of Japan. Ser. II.*

Jiang, H., and E. J. Zipser, 2010: Contribution of tropical cyclones to the global precipitation from eight seasons of TRMM data: Regional, seasonal, and interannual variations. *Journal of climate*, **23,** 1526-1543.

Jiang, H., C. Liu, and E. J. Zipser, 2011: A TRMM-based tropical cyclone cloud and precipitation feature database. *Journal of applied meteorology and climatology*, **50,** 1255-1274.

Kam, J., J. Sheffield, X. Yuan, and E. F. Wood, 2013: The Influence of Atlantic Tropical Cyclones on Drought over the Eastern US (1980-2007), J. Climate, 26 (10), 3067-3086.

Kim, D., and Coauthors, 2018: Process-oriented diagnosis of tropical cyclones in high-resolution GCMs. *Journal of Climate*, 31, 1685-1702.

Khouakhi, A., G. Villarini, and G. A. Vecchi, 2017: Contribution of tropical cyclones to rainfall at the global scale. *Journal of Climate*, **30,** 359-372.

Klotzbach, P.J., S.G. Bowen, R. Pielke Jr., and M. Bell, Continental U.S. hurricane landfall frequency and associated damage: Observations and future risks, Bulletin of the American Meteorological Society, 99(7), 1359-1376, 2018.

Knapp, K. R., M. C. Kruk, D. H. Levinson, H. J. Diamond, and C. J. Neumann, 2010: The International Best Track Archive for Climate Stewardship (IBTrACS). *Bulletin of the American Meteorological Society*, **91,** 363-376.

Knight, D. B., and R. E. Davis, 2009: Contribution of tropical cyclones to extreme rainfall events in the southeastern United States. *Journal of Geophysical Research: Atmospheres*, **114**.
Lin, Y., M. Zhao, and M. Zhang, 2015: Tropical cyclone rainfall area controlled by relative sea surface temperature. *Nature communications*, **6,** 1-7.
Liu, M., G. A. Vecchi, J. A. Smith, and H. Murakami, 2018: Projection of landfalling–tropical cyclone rainfall in the Eastern United States under anthropogenic warming. *Journal of Climate*, **31,** 7269-7286.
Liu, M., G. A. Vecchi, J. A. Smith, and T. R. Knutson, 2019: Causes of large projected increases in hurricane precipitation rates with global warming. *npj Climate and Atmospheric Science*, **2,** 38.
Luitel, B., G. Villarini, and G.A. Vecchi, Verification of the skill of numerical weather prediction models in forecasting rainfall from U.S. landfalling tropical cyclones, Journal of Hydrology, 556, 1026-1037, 2018.
Manganello, J. V., and Coauthors, 2012: Tropical cyclone climatology in a 10-km global atmospheric GCM: toward weather-resolving climate modeling. Journal of Climate, 25, 3867-3893.
Miniussi, A., G. Villarini, and M. Marani, Analyses through the metastatistical extreme value distribution identify contributions of tropical cyclones to rainfall extremes in the eastern US, Geophysical Research Letters, 47(7), e2020GL087238, 1-9, 2020.
Moon, Y., and Coauthors, 2020: Azimuthally averaged wind and thermodynamic structures of tropical cyclones in global climate models and their sensitivity to horizontal resolution. *Journal of Climate*, **33,** 1575-1595.
Murakami, H., and Coauthors, 2015: Simulation and prediction of category 4 and 5 hurricanes in the high-resolution GFDL HiFLOR coupled climate model. Journal of Climate, 28, 9058-9079.
Nguyen, L. T., R. F. Rogers, and P. D. Reasor, 2017: Thermodynamic and kinematic influences on precipitation symmetry in sheared tropical cyclones: Bertha and Cristobal (2014). *Monthly Weather Review*, **145,** 4423-4446.
NOAA National Centers for Environmental Information (NCEI) U.S. Billion-Dollar Weather and Climate Disasters (2020). https://www.ncdc.noaa.gov/billions/, DOI: 10.25921/stkw-7w73
Peduzzi, P., B. Chatenoux, H. Dao, A. De Bono, C. Herold, J. Kossin, F. Mouton, and O. Nordbeck, Global trends in tropical cyclone risk, Nature Climate Change, 2, 289-294, 2012.
Prat, O. P., and B. R. Nelson, 2013a: Precipitation contribution of tropical cyclones in the southeastern United States from 1998 to 2009 using TRMM satellite data. *Journal of Climate*, **26,** 1047-1062.
——, 2013b: Mapping the world's tropical cyclone rainfall contribution over land using the TRMM Multi-satellite Precipitation Analysis. *Water Resources Research*, **49,** 7236-7254.
——, 2016: On the link between tropical cyclones and daily rainfall extremes derived from global satellite observations. Journal of Climate, 29, 6127-6135.
Rappaport, E.N., Fatalities in the United States from Atlantic tropical cyclones, 2014: New data and interpretation, *Bulletin of the American Meteorological Society*, **95(3)**, 341-346.
Reed, K. A., A. Standfield, M. F. Wehner, and C. M. Zarzycki, 2018: The human influence on Hurricane Florence. *website) accessed October*.
Rios Gaona, M.F., G. Villarini, W. Zhang, and G.A. Vecchi, The added value of IMERG in characterizing rainfall in tropical cyclones, *Atmospheric Research*, 209, 95-102, 2018.

Risser, M. D., and M. F. Wehner, 2017: Attributable human-induced changes in the likelihood and magnitude of the observed extreme precipitation during Hurricane Harvey. *Geophysical Research Letters*, **44,** 12,457-412,464.

Roberts, C. D., R. Senan, F. Molteni, S. Boussetta, M. Mayer, and S. P. Keeley, 2018: Climate model configurations of the ECMWF-Integrated Forecasting System (ECMWF-IFS cycle 43r1) for HighResMIP. *Geoscientific model development*, **11,** 3681-3712.

Roberts, C. D., R. Senan, F. Molteni, S. Boussetta, S. Keeley, 2017a: ECMWF ECMWF-IFS-LR model output prepared for CMIP6 HighResMIP. Version 20170915.Earth System Grid Federation. https://doi.org/10.22033/ESGF/CMIP6.2463

Roberts, C. D., R. Senan, F. Molteni, S. Boussetta, S. Keeley, 2017b: ECMWF ECMWF-IFS-HR model output prepared for CMIP6 HighResMIP. Version 20170915.Earth System Grid Federation. https://doi.org/10.22033/ESGF/CMIP6.2461

Roberts, M. J., and Coauthors, 2015: Tropical cyclones in the UPSCALE ensemble of high-resolution global climate models. Journal of Climate, 28, 574-596.

Roberts, M., 2017a: MOHC HadGEM3-GC31-LM model o 1008 utput prepared for CMIP6 HighResMIP. Version 20170906.Earth System Grid Federation. https://doi.org/10.22033/ESGF/CMIP6.1321

Roberts, M., 2017b: MOHC HadGEM3-GC31-MM model output prepared for CMIP6 HighResMIP. Version 20180818.Earth System Grid Federation. https://doi.org/10.22033/ESGF/CMIP6.1902

Roberts, M., 2017c: MOHC HadGEM3-GC31-HM model output prepared for CMIP6 HighResMIP. Version 20170831.Earth System Grid Federation.https://doi.org/10.22033/ESGF/CMIP6.446

Roberts, M. J., and Coauthors, 2019a: Description of the resolution hierarchy of the global coupled HadGEM3-GC313-GC3.1 model as used in CMIP6 HighResMIP experiments. *Geosci. Model Dev.*, **12,** 4999-5028.

Roberts, M. J., 2019b: CMIP6 HighResMIP: Tropical storm tracks as calculated by the TRACK algorithm. Centre for Environmental Data Analysis, 2019. http://catalogue.ceda.ac.uk/uuid/0b42715a7a804290afa9b7e31f5d7753

Roberts, M. J., and Coauthors, 2020: Impact of model resolution on tropical cyclone simulation using the HighResMIP-PRIMAVERA multi-model ensemble. *Journal of Climate*, **33**, 2557-2583.

Scoccimarro, E., S. Gualdi, G. Villarini, G. A. Vecchi, M. Zhao, K. Walsh, and A. Navarra, 2014: Intense precipitation events associated with landfalling tropical cyclones in response to a warmer climate and increased CO2. *Journal of climate*, **27,** 4642-4654.

Scoccimarro, E., A. Bellucci, D. Peano, 2017a: CMCC CMCC-CM2-HR4 model output prepared for CMIP6 HighResMIP. Version YYYYMMDD[1].Earth System Grid Federation. https://doi.org/10.22033/ESGF/CMIP6.1359

Scoccimarro, E., A. Bellucci, D. Peano, 2017b: CMCC CMCC-CM2-VHR4 model output prepared for CMIP6 HighResMIP. Version YYYYMMDD[1].Earth System Grid Federation. https://doi.org/10.22033/ESGF/CMIP6.1367

Scoccimarro, E., G. Villarini, S. Gualdi, A. Navarra, G. Vecchi, K. Walsh, and M. Zhao, 2017c: Tropical cyclone rainfall changes in a warmer climate. *Hurricanes and Climate Change*, Springer, 243-255.

Scoccimarro E., Gualdi S., Bellucci A. , Peano D., Cherchi A., Vecchi G.A. , Navarra A. 2020: The typhoon-induced drying of the Maritime Continent. PNAS doi: 10.1073/pnas.1915364117.

Shepherd, J. M., A. Grundstein, and T. L. Mote, 2007: Quantifying the contribution of tropical cyclones to extreme rainfall along the coastal southeastern United States. *Geophysical Research Letters*, **34**.

Tang, X., W.-C. Lee, and M. Bell, 2014: A squall-line-like principal rainband in Typhoon Hagupit (2008) observed by airborne Doppler radar. *Journal of the Atmospheric Sciences*, **71,** 2733-2746.

Taylor, K.E., D. Williamson and F. Zwiers, 2000: The sea surface temperature and sea ice concentration boundary conditions for AMIP II simulations. In PCMDI Report 60, Program for Climate Model Diagnosis and Intercomparison, Lawrence Livermore National Laboratory, 25 pp.

Touma, D., S. Stevenson, S. J. Camargo, D. E. Horton, and N. S. Diffenbaugh, 2019: Variations in the intensity and spatial extent of tropical cyclone precipitation. *Geophysical Research Letters*, **46**, 13992-14002.

Van Oldenborgh, G. J., and Coauthors, 2017: Attribution of extreme rainfall from Hurricane Harvey, August 2017. *Environmental Research Letters*, **12,** 124009.

Vecchi, G. A., and Coauthors, 2019: Tropical cyclone sensitivities to CO2 doubling: roles of atmospheric resolution, synoptic variability and background climate changes. *Climate Dynamics*, **53,** 5999-6033.

Villarini, G., J. A. Smith, M. L. Baeck, T. Marchok, and G. A. Vecchi, 2011: Characterization of rainfall distribution and flooding associated with U.S. landfalling tropical cyclones: Analyses of Hurricanes Frances, Ivan, and Jeanne (2004). *Journal of Geophysical Research: Atmospheres*, **116**.

Villarini, G., R. Goska, J.A. Smith, and G.A. Vecchi, North Atlantic tropical cyclones and U.S. flooding, Bulletin of the American Meteorological Society, 95(9), 1381-1388, 2014a.

Villarini, G., and R. F. Denniston, 2016: Contribution of tropical cyclones to extreme rainfall in Australia. *International Journal of Climatology*, **36,** 1019-1025.

Villarini, G., and Coauthors, 2014b: Sensitivity of tropical cyclone rainfall to idealized global-scale forcings. *Journal of climate*, **27,** 4622-4641.

Voldoire, A., and Coauthors, 2019: Evaluation of CMIP6 DECK Experiments With CNRM-CM6-1. *Journal of Advances in Modeling Earth Systems*, **11,** 2177-2213.

Vanniere, B., and Coauthors, The moisture budget of tropical cyclones: large scale environmental constraints and sensitivity to model horizontal resolution, Journal of Climate, 33, 8457-8474.

Voldoire, A., 2018: CNRM-CERFACS CNRM-1092 CM6-1 model output prepared for CMIP6 HighResMIP. Earth System Grid Federation. http://cera1094www.dkrz.de/WDCC/meta/CMIP6/CMIP6.HighResMIP.CNRM-CERFACS.CNRM1095CM6-1

Voldoire, A., 2017: CNRM-CERFACS CNRM-CM6-1-HR model output prepared for CMIP6 HighResMIP. Earth System Grid Federation. http://cera1098www.dkrz.de/WDCC/meta/CMIP6/CMIP6.HighResMIP.CNRM-CERFACS.CNRM1099CM6-1-HR

von Storch, J.-S., and Coauthors, 2017: MPI-M MPI-ESM1.2-HR model output prepared for CMIP6 HighResMIP. Earth System Grid Federation.

http://cera1105www.dkrz.de/WDCC/meta/CMIP6/CMIP6.HighResMIP.MPI-M.MPI-ESM1-2-HR

von Storch, J.-S., and Coauthors, 2019: MPI-M MPI-ESM1.2-XR model output prepared for CMIP6 HighResMIP. Earth System Grid Federation. http://cera1108www.dkrz.de/WDCC/meta/CMIP6/CMIP6.HighResMIP.MPI-M.MPI-ESM1-2-XR

Wang, S. S., L. Zhao, J.-H. Yoon, P. Klotzbach, and R. R. Gillies, 2018: Quantitative attribution of climate effects on Hurricane Harvey's extreme rainfall in Texas. *Environmental Research Letters*, **13,** 054014.

Wang, Y., K.-H. Lee, Y. Lin, M. Levy, and R. Zhang, 2014: Distinct effects of anthropogenic aerosols on tropical cyclones. *Nature Climate Change*, **4,** 368-373.

Wehner, M. F., and Coauthors, 2014: The effect of horizontal resolution on simulation quality in the C ommunity A tmospheric M odel, CAM 5.1. Journal of Advances in Modeling Earth Systems, 6, 980-997.

Wright, D. B., T. R. Knutson, and J. A. Smith, 2015: Regional climate model projections of rainfall from US landfalling tropical cyclones. *Climate dynamics*, **45,** 3365-3379.

Yu, Z., Y. Wang, H. Xu, N. Davidson, Y. Chen, Y. Chen, and H. Yu, 2017: On the relationship between intensity and rainfall distribution in tropical cyclones making landfall over China. *Journal of Applied Meteorology and Climatology*, **56,** 2883-2901.

Zhang, M., X. Chen, M. Kumar, M. Marani, and M. Goralczyk (2017). Hurricanes and tropical storms: A necessary evil to ensure water supply? Hydrological Processes, 31, 4414–4428. https://doi.org/10.1002/hyp.11371

Zhang, W., and Coauthors, 2015: Improved Simulation of Tropical Cyclone Responses to ENSO in the Western North Pacific in the High-Resolution GFDL HiFLOR Coupled Climate Model. *Journal of Climate*, 29, 1391-1415.

Zhang, W., G. Villarini, G. A. Vecchi, and J. A. Smith, 2018: Urbanization exacerbated the rainfall and flooding caused by hurricane Harvey in Houston. *Nature*, **563,** 384-388.

Zhang, W., G. Villarini, G. A. Vecchi, and H. Murakami, 2019: Rainfall from tropical cyclones: high-resolution simulations and seasonal forecasts. *Climate Dynamics*, **52,** 5269-5289.

Zhao, C., Y. Lin, F. Wu, Y. Wang, Z. Li, D. Rosenfeld, and Y. Wang, 2018: Enlarging rainfall area of tropical cyclones by atmospheric aerosols. Geophysical Research Letters, 45, 8604-8611.

Zhao, M., I. M. Held, S.-J. Lin, and G. A. Vecchi, 2009: Simulations of global hurricane climatology, interannual variability, and response to global warming using a 50-km resolution GCM. Journal of Climate, 22, 6653-6678.

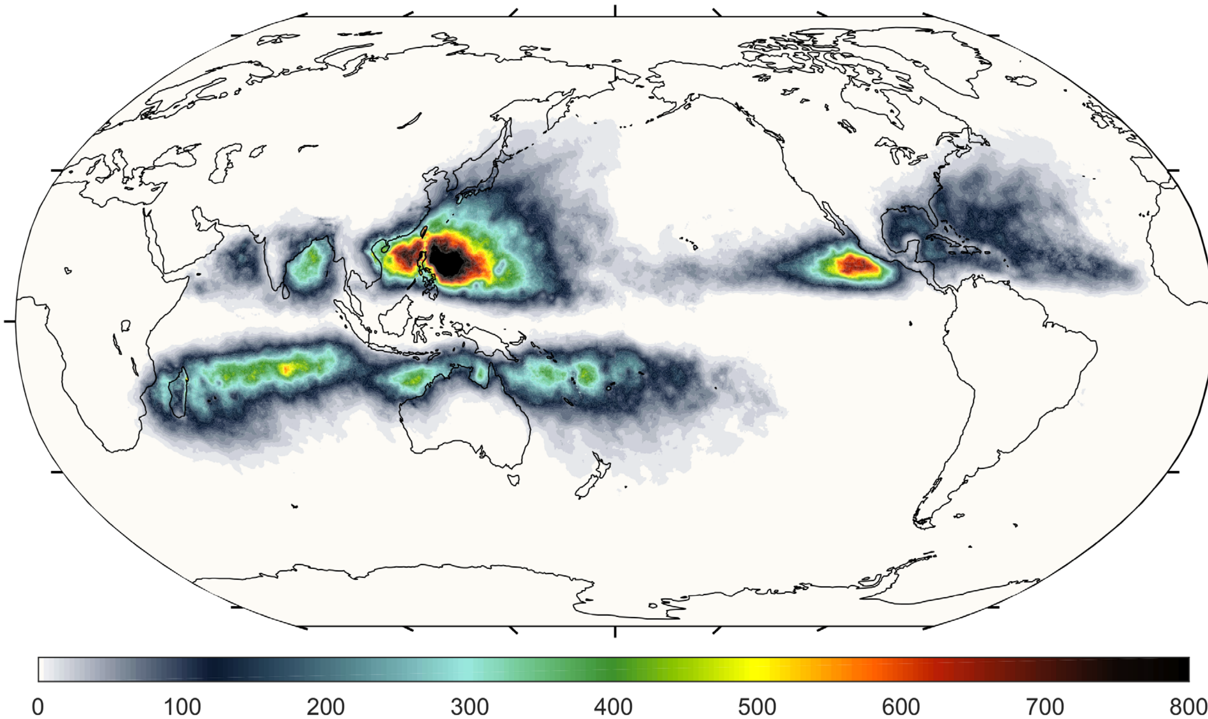

Figure 1 Annual average TC rainfall (unit: mm/year) in observations.

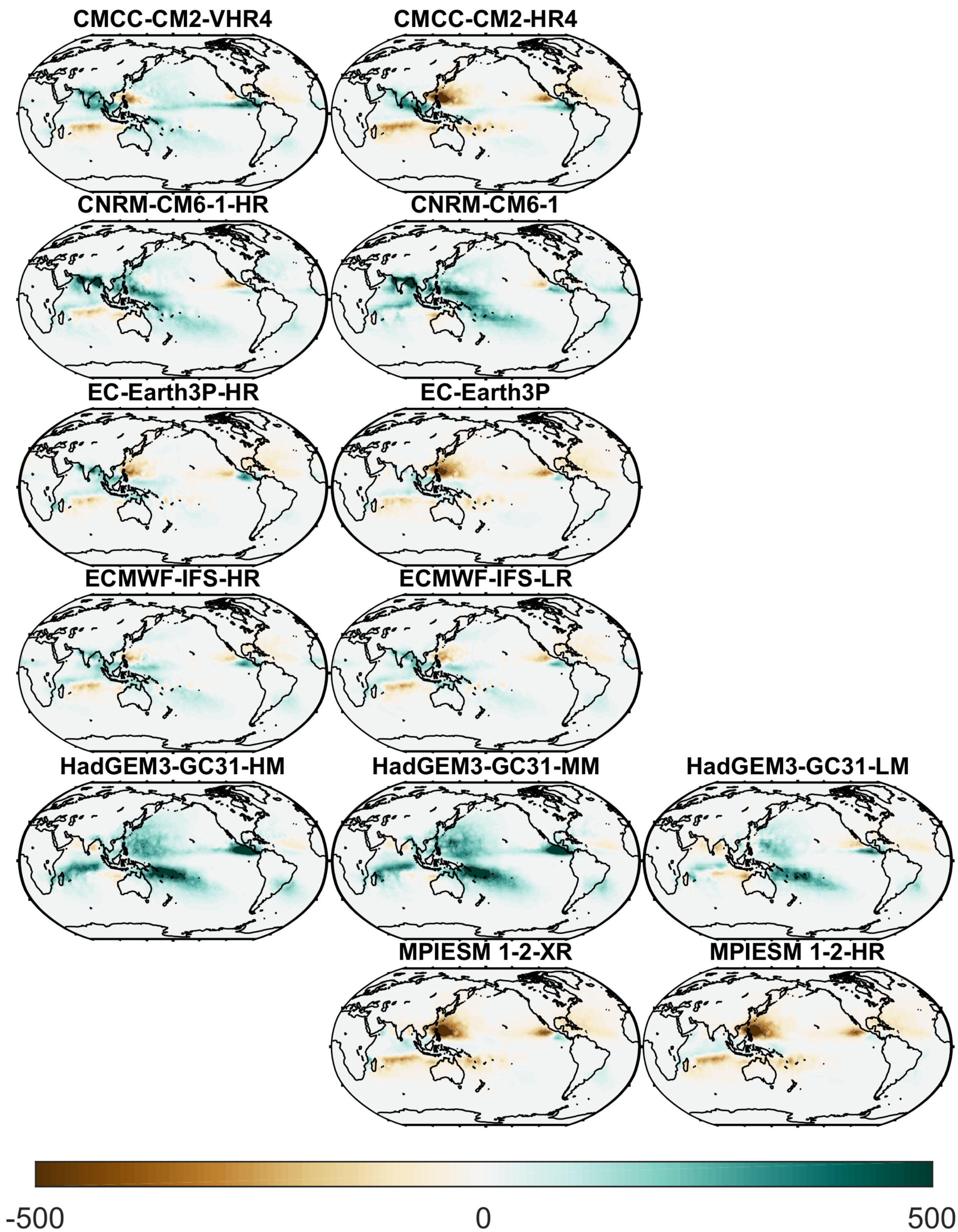

Figure 2. Differences in annual average TC rainfall (unit: mm/year) between observations and climate models archived in the PRIMAVERA Project (model minus observations).

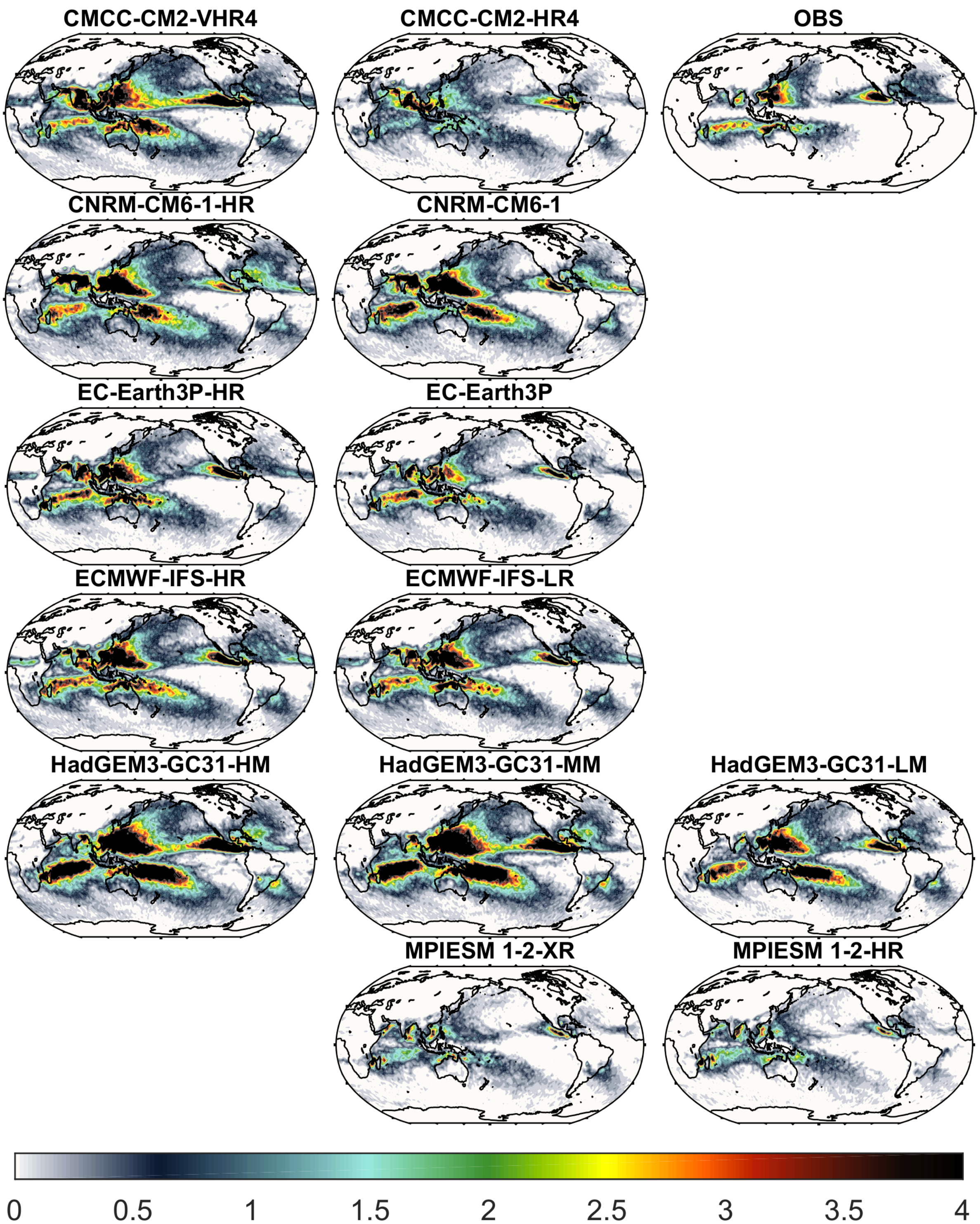

Figure 3. Annual average TC track density obtained by binning TC tracks into 2×2 spatial boxes in observations and climate models archived in the PRIMAVERA Project.

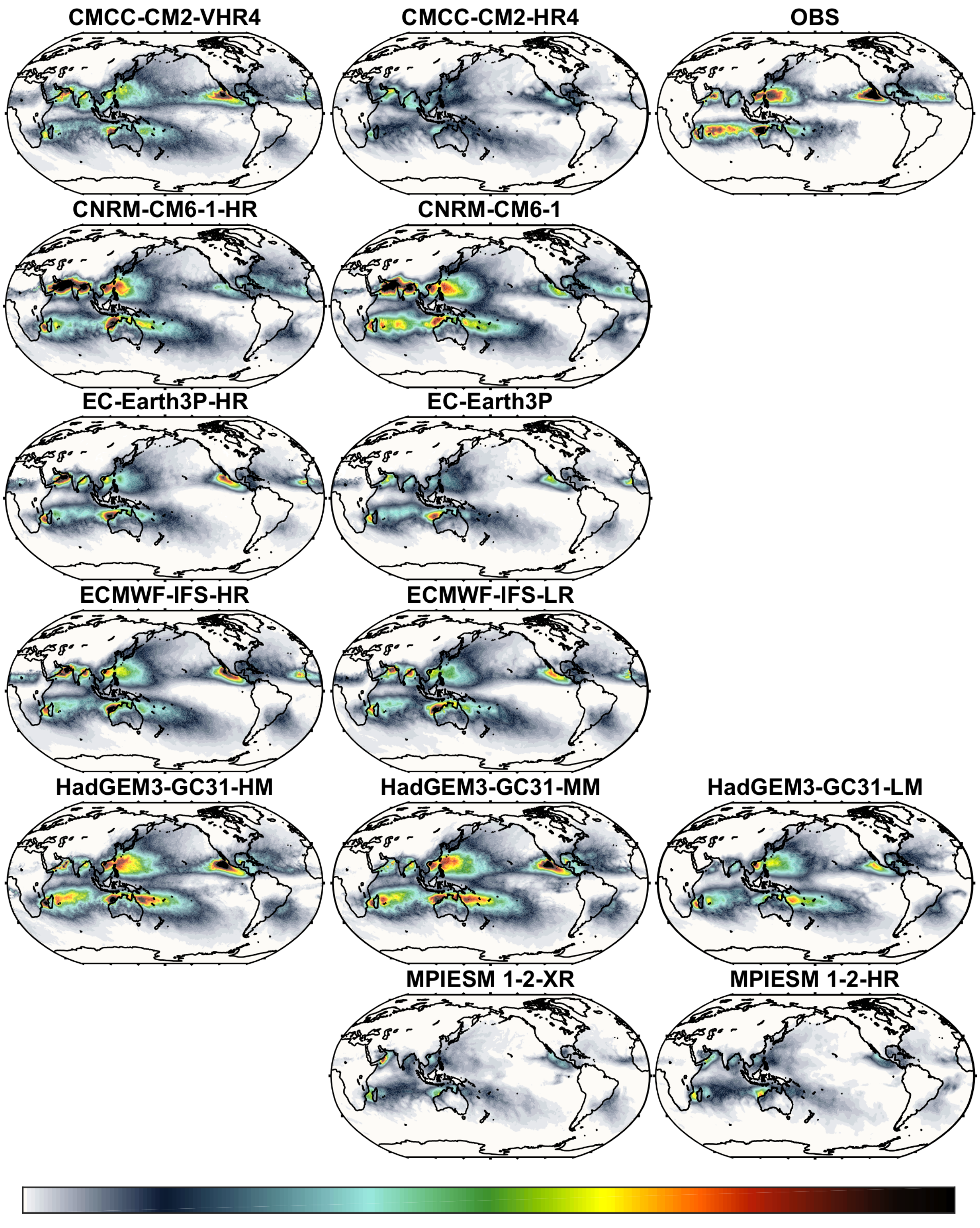

Figure 4. Percentage contribution of TC rainfall to total rainfall (unit: %) in observations and climate models archived in the PRIMAVERA Project.

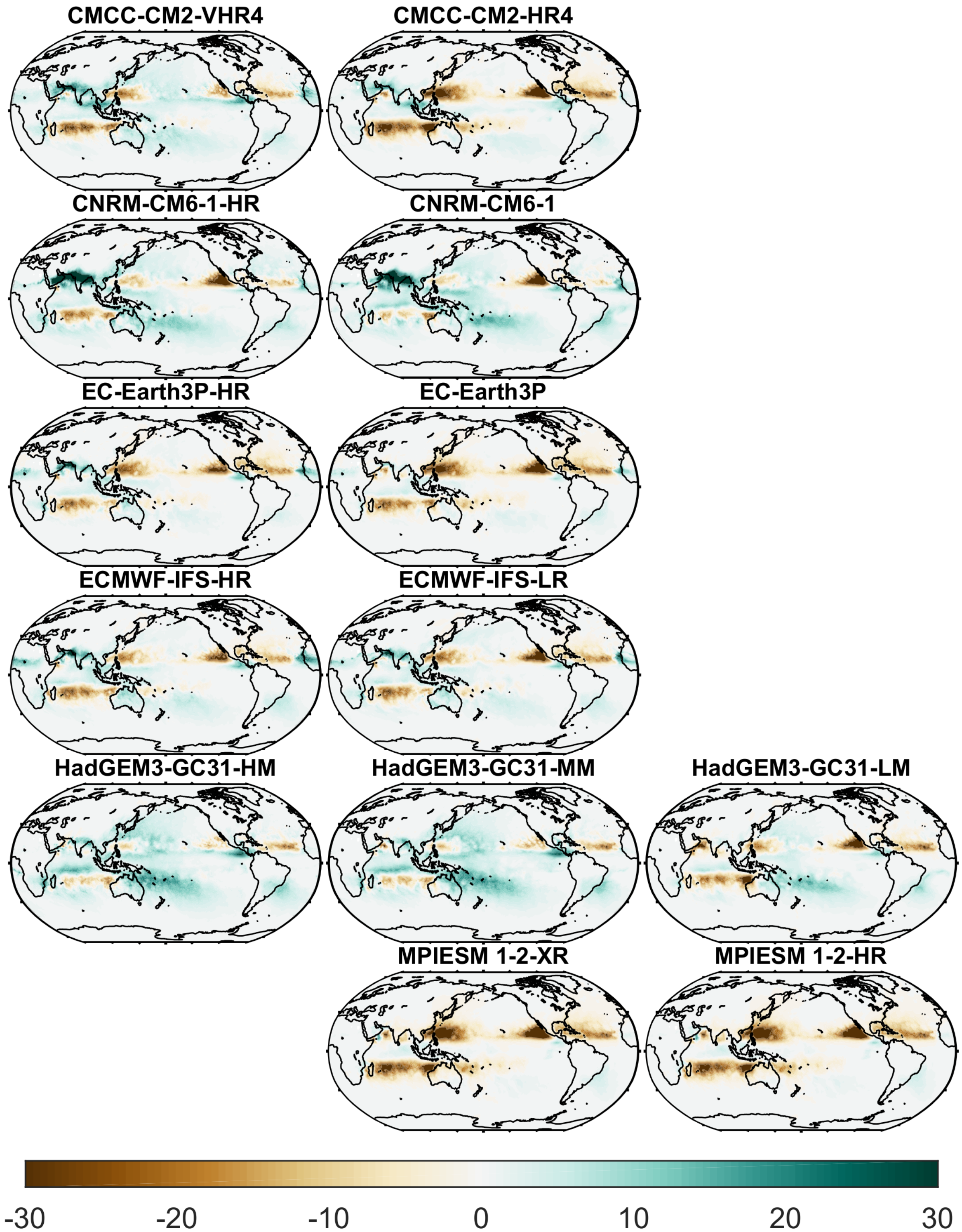

Figure 5. Bias (model minus observations) in the percentage contribution of TC rainfall to total rainfall (unit: %) in the models.

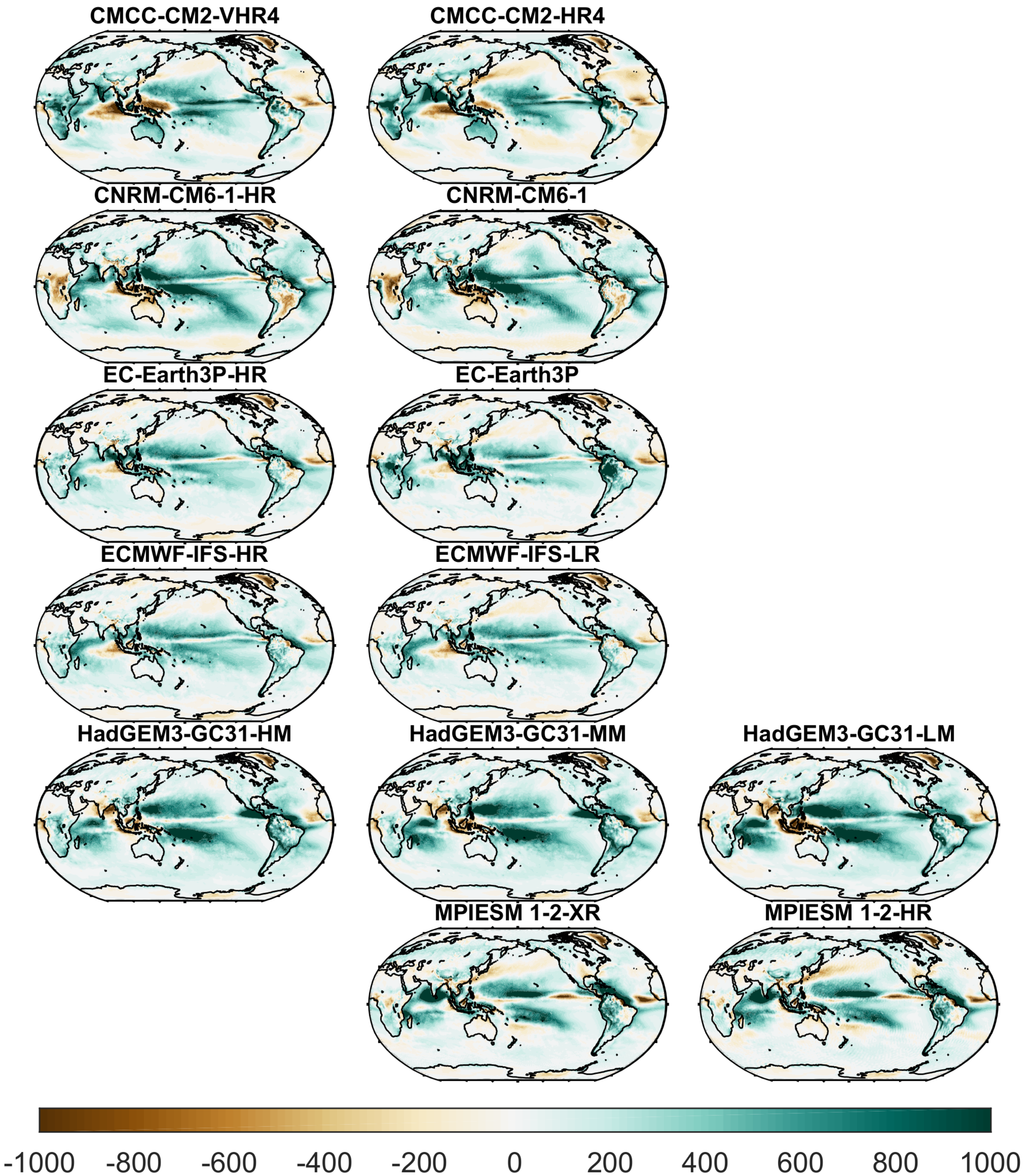

Figure 6. Bias (model minus observations) in total rainfall (unit: mm/year) in the models.

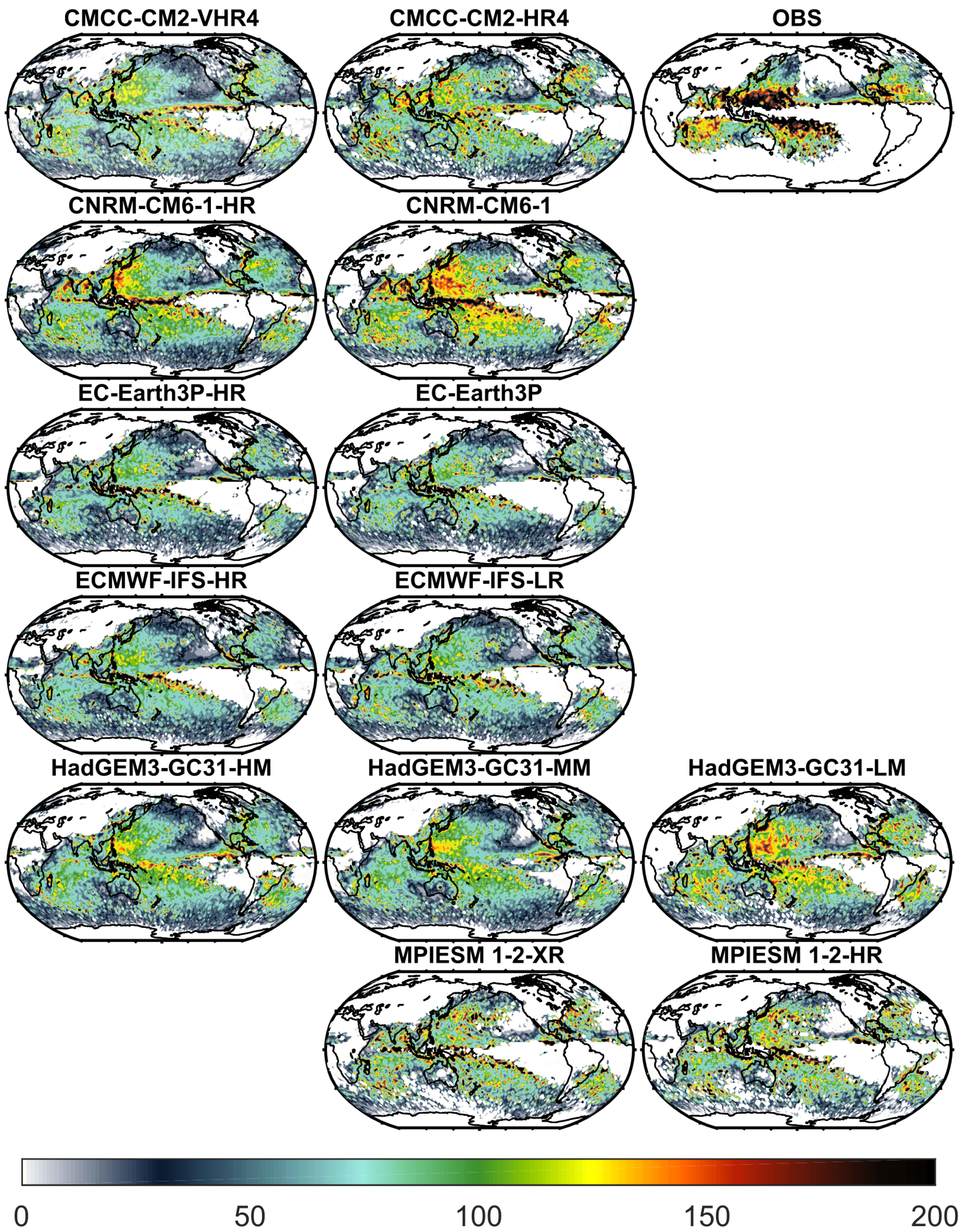

Figure 7. Average rainfall divided by TC track density (unit: mm) in observations and climate models archived in the PRIMAVERA Project. Average rainfall per TC track density represent the annual total TC rainfall divided by TC track density obtained by binning TC tracks into 2×2 spatial boxes.

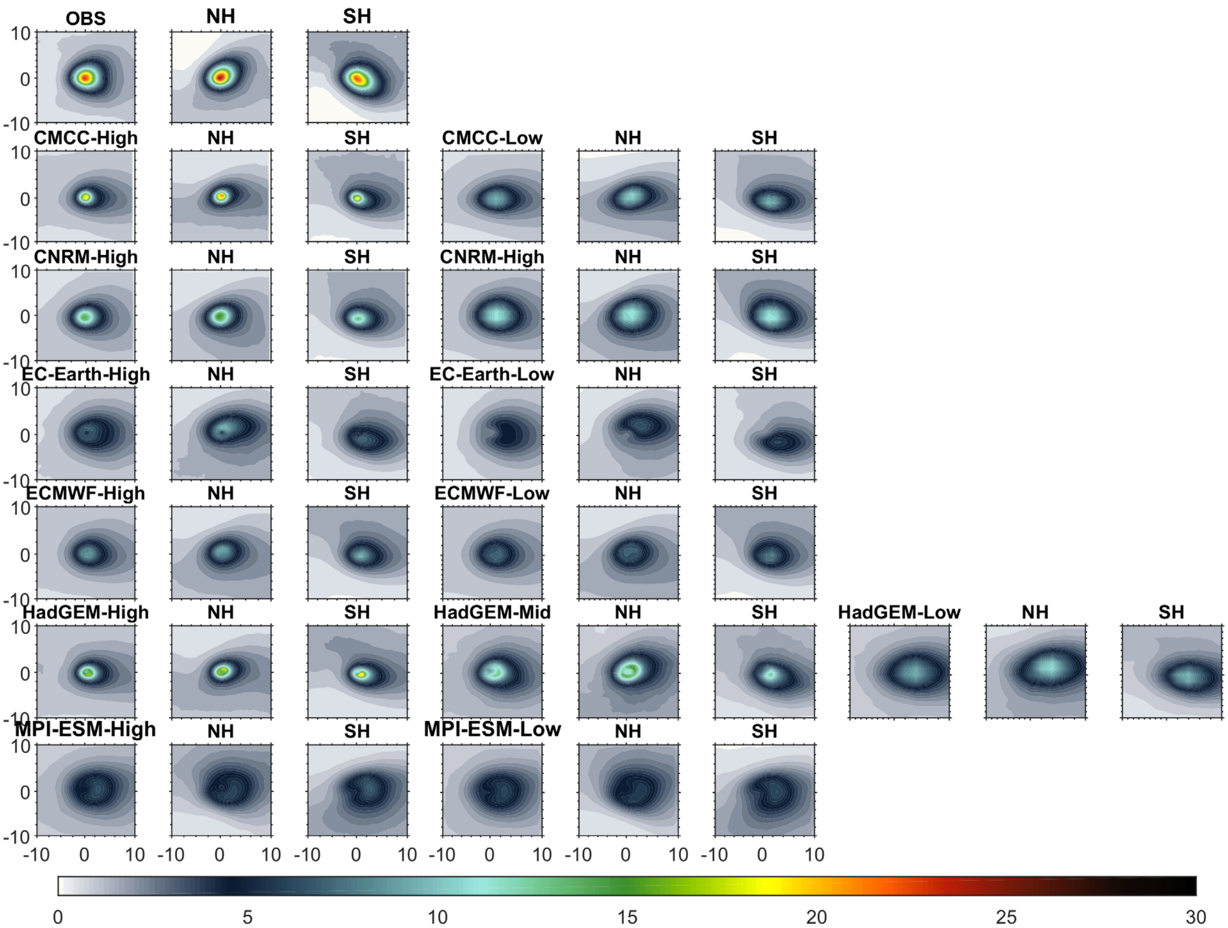

Figure 8. Composite 6-hour TC Rainfall (unit: mm) over the ocean & land in observations and climate models archived in the PRIMAVERA Project. The model resolution drops from left (columns 1-3) to right (columns 4-6 and 7-9). Every group of three columns represents the composite for all the storms, those in the northern hemisphere and those in the southern hemisphere.

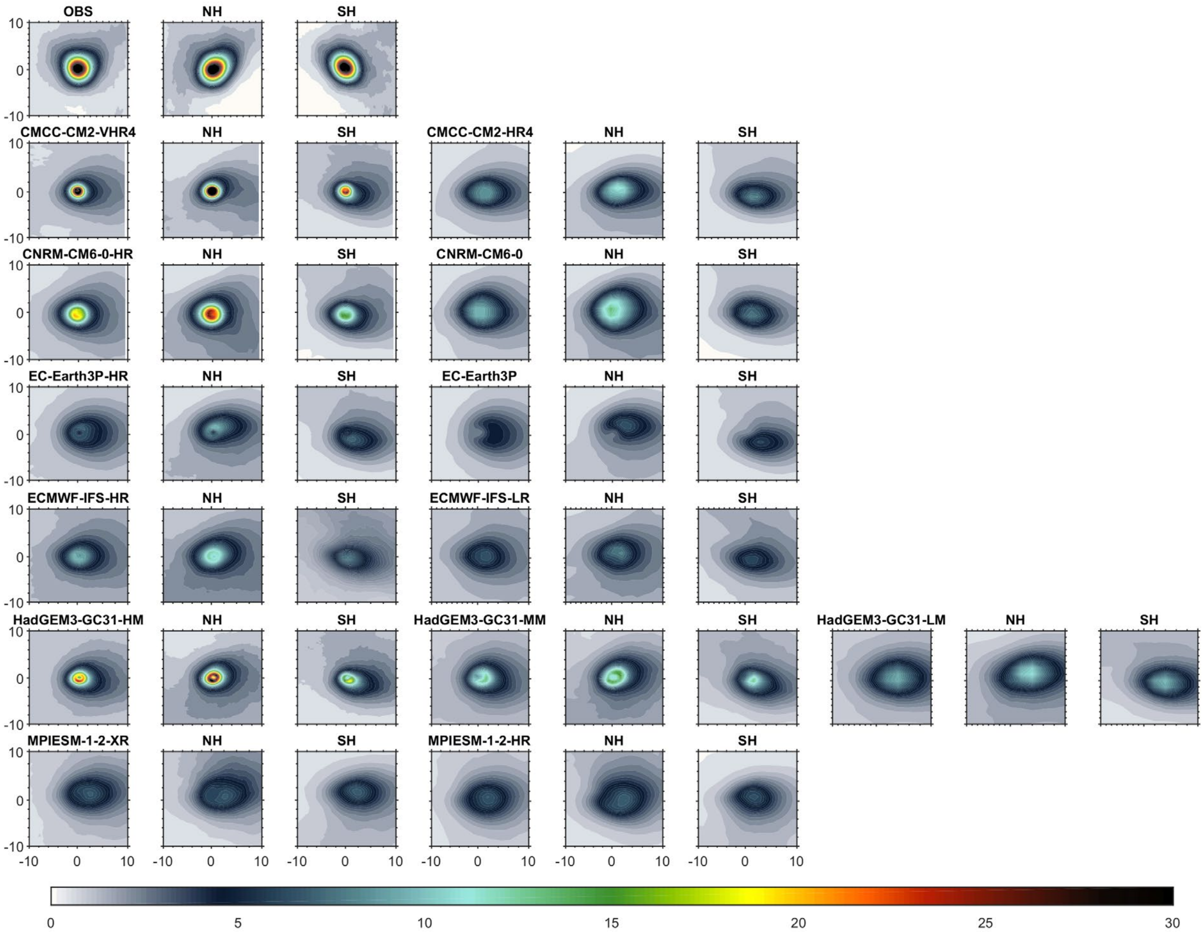

Figure 9. Composite 6-hour TC rainfall (unit: mm) across the 200 TCs with strongest intensity (sea level pressure) over the land and ocean in observations and climate models archived in the PRIMAVERA Project during 1980-2010. The model resolution drops from left (columns 1-3) to right (columns 4-6 and 7-9).

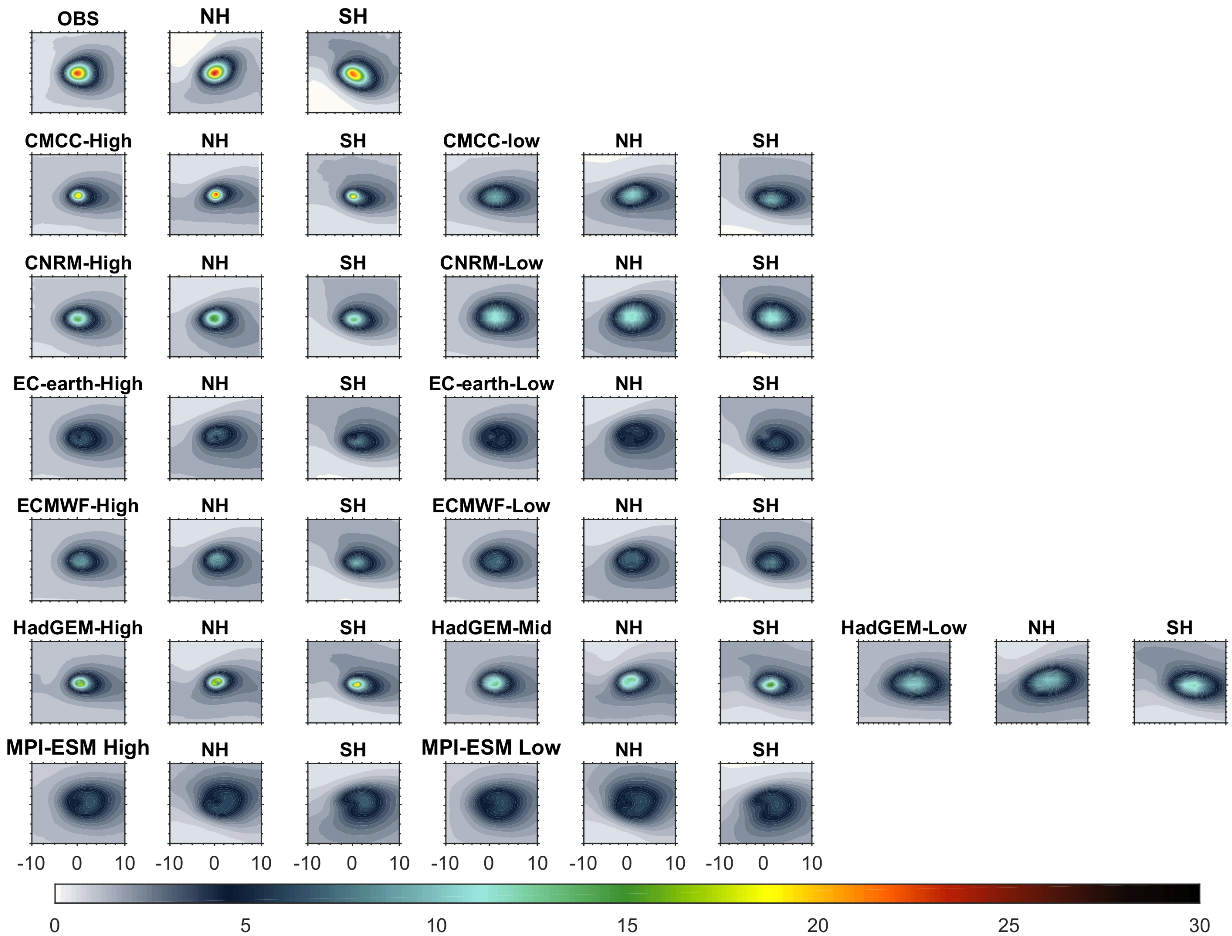

Figure 10. Same as Figure 8 but over ocean.

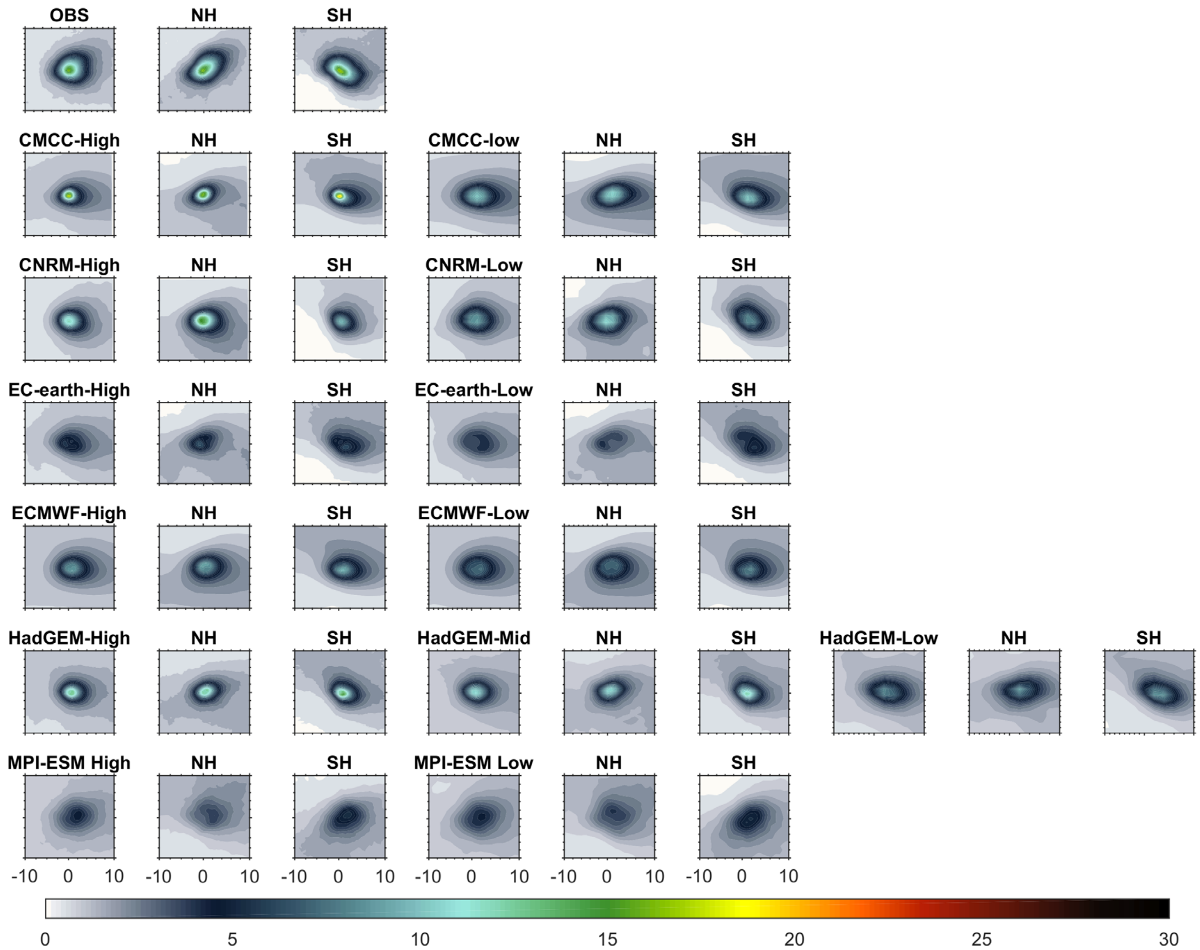

Figure 11. Same as Figure 8 but over land.

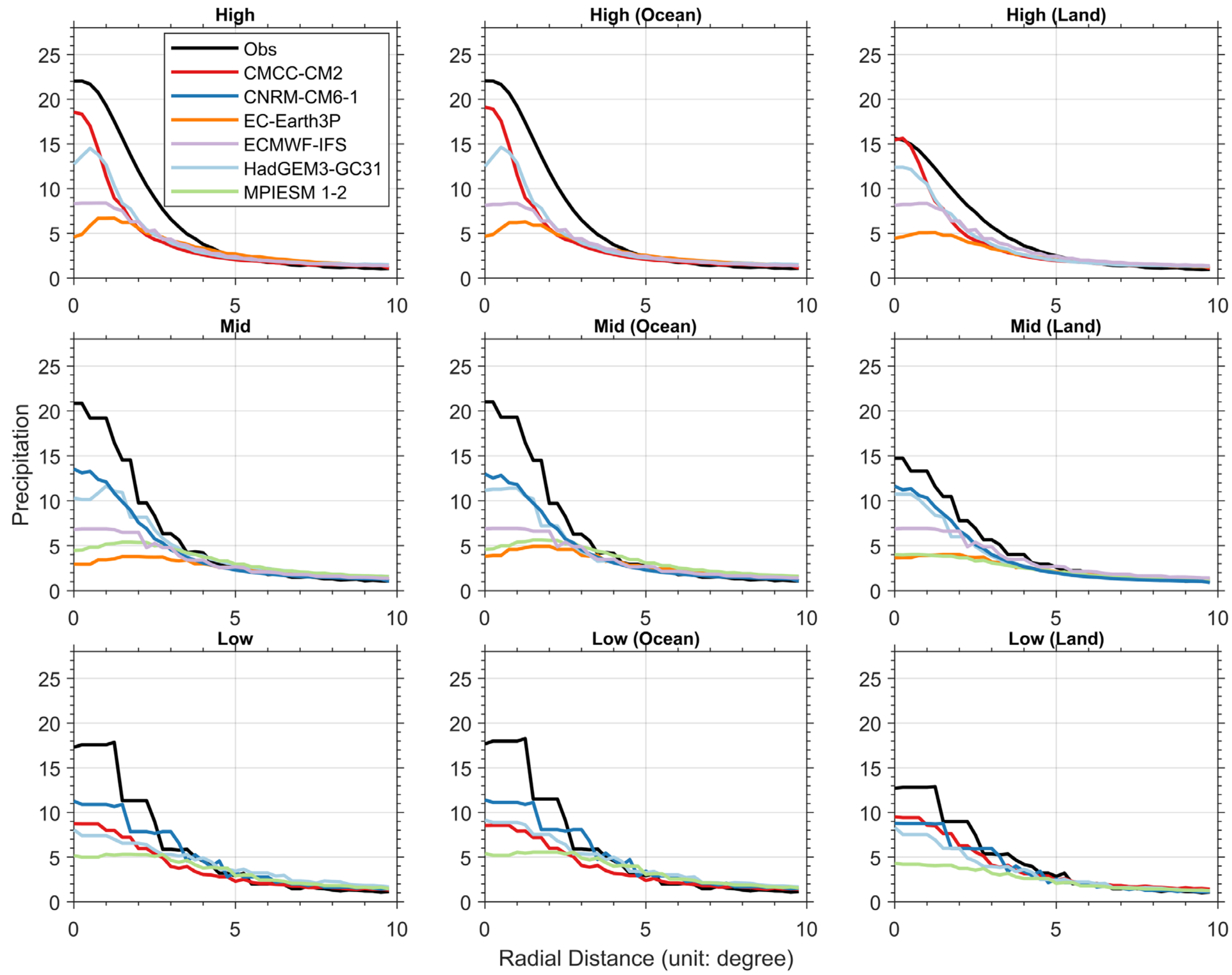

Figure 12. Radial profile of composite 6-hour TC rainfall (unit: mm) in observations and models grouped into high-, mid-, and low-resolution climate models**.** The spatial resolution of observed TC rainfall is re-gridded to each group (High, Mid and Low resolution) of the models.

Table 1. Spatial grids of the climate model outputs in high-, middle- and low-resolution groups used in this study. While ECMWF IFS data provided to HighResMIP are based on a reduced-resolution regular grid, the original ECMWF-IFS output uses the cubic octahedral reduced Gaussian grid, with resolutions of Tco399 (~25 km) and Tco199 (~50 km) for the HR and LR configurations, respectively.

Model	High	Middle/Medium	Low
CMCC-CM2	1152×768		288×192
CNRM-CM6-1		720×360	256×128
EC-Earth3P	1024×512	512×256	
ECMWF-IFS	720×361	360×181	
HadGEM3-GC313	1024×768	432×324	192×144
MPI-ESM1-2		768×384	384×192

Table 2 Definitions of basin boundaries

Basins	Boundary
Western North Pacific (WNP)	0-60°N, 100°E-180
Eastern North Pacific (ENP)	0-60°N, 180-100°W
North Atlantic (NA)	0-60°N, 100°W-0
North Indian Ocean (NI)	0-45°N, 45°E-100°E
South-West Indian Ocean (SI)	0-40°S, 0-90°E
South Pacific & Australia (SP)	0-40°S, 90°E-120°W
South Atlantic (SA)	0-60°S, 60°W-0

Table 3 Correlation between observed and simulated tropical cyclone rainfall across the globe and in different basins.

	Globe	WNP	ENP	NA	NI	SI	SP
CMCC-CM2-VHR4	0.77	0.87	0.77	0.68	0.83	0.80	0.76
CMCC-CM2-HR4	0.54	0.62	0.59	0.41	0.77	0.80	0.61
CNRM-CM6-1-HR	0.80	0.94	0.29	0.80	0.70	0.84	0.79
CNRM-CM6-1	0.81	0.89	0.41	0.82	0.74	0.88	0.72
EC-Earth3P-HR	0.85	0.89	0.37	0.77	0.89	0.86	0.90
EC-Earth3P	0.83	0.85	0.33	0.78	0.92	0.88	0.89
ECMWF-IFS-HR	0.87	0.92	0.71	0.79	0.87	0.84	0.85
ECMWF-IFS-LR	0.86	0.92	0.66	0.80	0.88	0.81	0.85
HadGEM3-GC31-HM	0.83	0.94	0.74	0.71	0.62	0.86	0.78
HadGEM3-GC31-MM	0.83	0.93	0.71	0.71	0.70	0.85	0.76
HadGEM3-GC31-LM	0.83	0.94	0.69	0.75	0.76	0.86	0.71
MPIESM 1-2-XR	0.67	0.68	0.26	0.64	0.81	0.73	0.81
MPIESM 1-2-HR	0.71	0.76	0.13	0.75	0.91	0.74	0.82

Table 4 Root mean square error (unit: mm) between observed and simulated tropical cyclone rainfall across the globe and in different basins.

	Globe	WNP	ENP	NA	NI	SI	SP
CMCC-CM2-VHR4	73.39	97.99	61.43	84.63	151.15	64.61	77.94
CMCC-CM2-HR4	79.44	152.37	14.90	80.66	140.61	83.06	74.72
CNRM-CM6-1-HR	95.27	136.22	27.57	46.58	280.06	61.12	67.15
CNRM-CM6-1	106.18	171.88	31.54	53.07	267.48	82.55	80.14
EC-Earth3P-HR	50.48	85.67	14.43	53.69	99.63	54.91	50.96
EC-Earth3P	54.26	125.33	13.08	51.90	40.53	51.50	42.83
ECMWF-IFS-HR	51.28	75.38	16.20	50.56	90.48	58.20	64.27
ECMWF-IFS-LR	49.17	75.97	15.91	44.59	93.09	62.63	61.00
HadGEM3-GC31-HM	129.29	159.11	59.40	161.02	75.63	151.65	143.76
HadGEM3-GC31-MM	130.32	173.13	56.98	151.07	68.51	145.72	147.59
HadGEM3-GC31-LM	76.46	96.64	25.58	62.46	45.38	70.04	96.37
MPIESM 1-2-XR	72.34	171.84	14.29	61.76	43.83	74.66	64.69
MPIESM 1-2-HR	69.57	167.61	14.15	57.32	31.24	72.98	61.12

Table 5 Correlation between observed and simulated tropical cyclone rainfall proportion across the globe and in different basins.

	Globe	WNP	ENP	NA	NI	SI	SP
CMCC-CM2-VHR4	0.80	0.86	0.88	0.85	0.71	0.79	0.87
CMCC-CM2-HR4	0.65	0.72	0.71	0.64	0.67	0.79	0.86
CNRM-CM6-1-HR	0.71	0.92	0.55	0.75	0.64	0.85	0.86
CNRM-CM6-1	0.75	0.92	0.53	0.73	0.72	0.93	0.88
EC-Earth3P-HR	0.82	0.91	0.57	0.78	0.80	0.88	0.95
EC-Earth3P	0.81	0.90	0.53	0.72	0.87	0.89	0.95
ECMWF-IFS-HR	0.80	0.93	0.83	0.74	0.78	0.85	0.89
ECMWF-IFS-LR	0.79	0.92	0.79	0.70	0.80	0.82	0.91
HadGEM3-GC31-HM	0.86	0.93	0.78	0.87	0.84	0.88	0.83
HadGEM3-GC31-MM	0.85	0.92	0.71	0.86	0.80	0.88	0.82
HadGEM3-GC31-LM	0.79	0.94	0.67	0.81	0.64	0.90	0.69
MPIESM 1-2-XR	0.69	0.70	0.08	0.64	0.77	0.77	0.89
MPIESM 1-2-HR	0.73	0.77	-0.05	0.67	0.83	0.77	0.93

Table 6 Root mean square error (unit: %) between observed and simulated tropical cyclone rainfall proportion across the globe and in different basins.

	Globe	WNP	ENP	NA	NI	SI	SP
CMCC-CM2-VHR4	5.10	5.90	3.41	5.32	9.66	7.93	6.43
CMCC-CM2-HR4	6.58	9.13	2.11	8.61	6.89	9.81	9.88
CNRM-CM6-1-HR	6.57	4.80	2.42	6.98	18.22	6.28	6.69
CNRM-CM6-1	6.26	4.85	2.50	6.97	16.71	4.66	6.14
EC-Earth3P-HR	4.80	6.20	2.41	6.70	7.95	6.47	4.18
EC-Earth3P	5.44	8.59	2.66	8.08	3.73	7.07	5.34
ECMWF-IFS-HR	4.99	4.70	1.77	6.78	8.36	7.26	5.79
ECMWF-IFS-LR	5.03	5.51	1.92	7.49	7.24	7.09	5.03
HadGEM3-GC31-HM	5.14	5.92	3.29	4.92	5.28	6.48	7.99
HadGEM3-GC31-MM	5.14	5.75	3.14	5.14	5.21	5.96	8.26
HadGEM3-GC31-LM	5.10	4.23	2.09	6.82	6.07	5.86	8.78
MPIESM 1-2-XR	6.87	10.79	2.86	9.43	4.82	9.46	9.41
MPIESM 1-2-HR	6.68	10.66	2.90	9.42	4.37	9.23	8.10

Tropical Cyclone Precipitation in the HighResMIP Atmosphere-only Experiments of the PRIMAVERA Project

Wei Zhang[1,2*], Gabriele Villarini[1], Enrico Scoccimarro[3], Malcolm Roberts[4], Pier Luigi Vidale[5], Benoıt Vanniere[5], Louis-Philippe Caron[6], Dian Putrasahan[7], Christopher Roberts[8], Retish Senan[8], and Marie-Pierre Moine[9]

[1] IIHR-Hydroscience & Engineering, The University of Iowa, Iowa City, Iowa, USA

[2]Department of Plants, Soils and Climate, Utah State University, Utah, USA

[3] Fondazione Centro Euro-Mediterraneo sui Cambiamenti Climatici, Bologna, Italy

[4] UK Meteorological Office, Exeter, UK

[5]National Centre for Atmospheric Science (NCAS), Department of Meteorology, University of Reading, Reading, UK

[6]Barcelona Supercomputing Center (BSC), Barcelona, Spain

[7]Max Planck Gesellschaft zur Foerderung der Wissenschaften E.V. (MPI-M), Hamburg, Germany

[8]European Centre for Medium-Range Weather Forecasts (ECMWF), Reading, UK

[9]Climat, Environnement, Couplages, Incertitudes (CECI), Universit´e de Toulouse, CNRS, Cerfacs, Toulouse, France

Table S1 Climatological frequencies of tropical cyclones (January-December, unit: mean storms/yr) in the globe and different basins in observations and the climate models.

	Globe	NH	SH	WNP	ENP	NA	NI	SI	SP	SA
Observations	91.6	59.6	32	24.5	19.9	11.9	3.3	14.9	17.1	0
CMCC-CM2-VHR4	148.4	82.8	65.6	33.7	21.3	15.9	11.9	10.3	45.4	9.9
CMCC-CM2-HR4	83.6	48.1	35.5	20.1	7.3	11.4	9.3	6.5	24.1	4.9
CNRM-CM6-1-HR	163	84.8	78.2	40.1	11.3	18.9	14.5	15.6	52.1	10.5
CNRM-CM6-1	167.4	86	81.4	42	13.4	17.6	13	19.7	52	9.7
EC-Earth3P-HR	95.2	48.8	46.4	25	8.2	7.5	8.1	10.5	28.6	7.3
EC-Earth3P	72.7	31.8	40.9	17.2	4.9	4.8	4.9	8.5	25.4	7
ECMWF-IFS-HR	133.1	65.9	67.2	34.7	10.3	12.1	8.8	13	41	13.2
ECMWF-IFS-LR	117.5	58.1	59.4	30.4	9	9.6	9.1	12.3	36.3	10.8
HadGEM3-GC31-HM	206.6	99.7	106.9	43.3	23.6	25.5	7.3	23	69.8	14.1
HadGEM3-GC31-MM	215.4	104.7	110.7	47.3	25.1	24.8	7.5	23.8	73	13.9
HadGEM3-GC31-LM	138.4	63.3	75.1	34.9	12.9	12.3	3.2	16.1	49.7	9.3
MPIESM 1-2-XR	47.3	19.6	27.7	7.8	4.6	3.3	3.9	6	15.6	6.1
MPIESM 1-2-HR	46.9	20.5	26.4	8.6	3.9	4.2	3.8	6.6	15.7	4.1

Table S2 Correlation between observed and simulated tropical cyclone rainfall per TC across the globe and in different basins.

	Globe	WNP	ENP	NA	NI	SI	SP
CMCC-CM2-VHR4	0.25	0.09	0.46	0.21	0.25	0.10	0.23
CMCC-CM2-HR4	0.18	0.08	0.22	0.08	0.20	0.09	0.19
CNRM-CM6-1-HR	0.28	0.19	0.46	0.19	0.32	0.03	0.11
CNRM-CM6-1	0.26	0.16	0.36	0.19	0.18	0.04	0.14
EC-Earth3P-HR	0.26	0.16	0.38	0.24	0.22	0.09	0.17
EC-Earth3P	0.28	0.19	0.34	0.23	0.28	0.07	0.27
ECMWF-IFS-HR	0.29	0.20	0.43	0.26	0.28	0.11	0.16
ECMWF-IFS-LR	0.30	0.16	0.47	0.24	0.36	0.09	0.19
HadGEM3-GC31-HM	0.28	0.17	0.38	0.24	0.27	0.18	0.29
HadGEM3-GC31-MM	0.26	0.17	0.47	0.14	0.36	0.11	0.12
HadGEM3-GC31-LM	0.21	0.15	0.50	0.10	0.16	0.02	0.07
MPIESM 1-2-XR	0.17	0.06	0.22	0.17	0.16	0.11	0.17
MPIESM 1-2-HR	0.23	0.11	0.36	0.22	0.26	0.10	0.24

Table S3 Root mean square error between observed and simulated tropical cyclone rainfall per TC across the globe and in different basins.

	Globe	**WNP**	**ENP**	**NA**	**NI**	**SI**	**SP**
CMCC-CM2-VHR4	122.0	133.0	123.8	87.4	138.7	97.6	126.3
CMCC-CM2-HR4	126.5	133.8	139.1	101.2	137.5	103.3	125.8
CNRM-CM6-1-HR	118.7	128.0	122.0	81.0	131.4	95.3	129.0
CNRM-CM6-1	118.1	127.7	127.1	86.2	137.9	92.7	130.1
EC-Earth3P-HR	126.5	136.4	132.6	87.1	152.7	103.7	128.8
EC-Earth3P	126.8	136.3	143.4	93.3	145.8	102.5	126.0
ECMWF-IFS-HR	122.4	133.1	123.9	86.2	143.3	99.7	129.5
ECMWF-IFS-LR	122.1	133.6	121.6	87.8	137.8	98.7	127.9
HadGEM3-GC31-HM	120.9	130.7	126.8	82.0	148.8	93.4	122.6
HadGEM3-GC31-MM	121.7	130.1	122.4	88.9	141.4	94.8	130.4
HadGEM3-GC31-LM	122.5	128.7	117.0	93.3	151.8	100.8	135.9
MPIESM 1-2-XR	138.4	147.3	149.7	116.2	148.9	111.3	145.0
MPIESM 1-2-HR	129.2	144.3	123.0	91.4	141.5	110.7	138.3

Table S4 Root mean square error and correlation between observed and simulated tropical cyclone rainfall across ocean and land.

	Cor (Ocean)	**Cor (Land)**	**RMSE(Ocean)**	**RMSE(Land)**
CMCC-CM2-VHR4	0.79	0.68	66.22	47.32
CMCC-CM2-HR4	0.57	0.51	76.33	36.06
CNRM-CM6-1-HR	0.83	0.67	84.74	64.69
CNRM-CM6-1	0.83	0.62	100.07	57.45
EC-Earth3P-HR	0.86	0.81	48.42	22.17
EC-Earth3P	0.83	0.78	53.15	19.15
ECMWF-IFS-HR	0.88	0.82	47.95	28.07
ECMWF-IFS-LR	0.87	0.83	46.61	24.76
HadGEM3-GC31-HM	0.83	0.79	126.41	48.80
HadGEM3-GC31-MM	0.83	0.80	128.95	40.77
HadGEM3-GC31-LM	0.84	0.83	76.46	18.41
MPIESM 1-2-XR	0.67	0.64	71.22	24.76
MPIESM 1-2-HR	0.72	0.66	68.45	24.08

Table S5 Root mean square error and correlation between observed and simulated tropical cyclone rainfall proportion across ocean and land.

	Cor (Ocean)	Cor (Land)	RMSE(Ocean)	RMSE(Land)
CMCC-CM2-VHR4	0.83	0.69	4.62	3.25
CMCC-CM2-HR4	0.71	0.58	6.45	2.39
CNRM-CM6-1-HR	0.79	0.64	5.27	5.67
CNRM-CM6-1	0.80	0.64	5.42	4.71
EC-Earth3P-HR	0.85	0.74	4.50	2.52
EC-Earth3P	0.84	0.77	5.38	1.62
ECMWF-IFS-HR	0.84	0.71	4.51	3.22
ECMWF-IFS-LR	0.82	0.78	4.78	2.46
HadGEM3-GC31-HM	0.87	0.83	4.85	2.68
HadGEM3-GC31-MM	0.86	0.82	4.89	2.50
HadGEM3-GC31-LM	0.80	0.78	5.04	1.66
MPIESM 1-2-XR	0.70	0.72	6.85	1.86
MPIESM 1-2-HR	0.74	0.74	6.66	1.77

Table S6 Root mean square error and correlation between observed and simulated tropical cyclone rainfall per TC across ocean and land.

	Cor (Ocean)	Cor (Land)	RMSE(Ocean)	RMSE(Land)
CMCC-CM2-VHR4	0.23	0.22	149.59	119.35
CMCC-CM2-HR4	0.16	0.11	153.68	130.84
CNRM-CM6-1-HR	0.29	0.25	144.20	120.22
CNRM-CM6-1	0.28	0.13	142.20	131.28
EC-Earth3P-HR	0.29	0.19	149.68	134.39
EC-Earth3P	0.25	0.20	157.39	136.33
ECMWF-IFS-HR	0.29	0.19	149.05	121.70
ECMWF-IFS-LR	0.31	0.26	146.64	123.05
HadGEM3-GC31-HM	0.31	0.18	146.65	126.26
HadGEM3-GC31-MM	0.30	0.13	146.91	129.38
HadGEM3-GC31-LM	0.25	0.04	144.65	136.30
MPIESM 1-2-XR	0.17	0.05	163.18	155.18
MPIESM 1-2-HR	0.20	0.17	161.12	145.98